

Structure and kinematics of candidate double-barred galaxies.[?]

A. V. Moiseev^{1??}, J. R. Valdes², and V. H. Chavushyan²

¹ Special Astrophysical Observatory, Nizhnij Arkhiz, Karachaevo-Cherkessia, 369167, Russia

² Instituto Nacional de Astrofísica Óptica y Electrónica, Apartado Postal 51 y 216, C. P. 72000, Puebla, Pue., Mexico

Received / accepted

Abstract. Results of optical and NIR spectral and photometric observations of a sample of candidate double-barred galaxies are presented. Velocity fields and velocity dispersion maps of stars and ionized gas, continuum and emission-line images were constructed from integral-field spectroscopy observations carried out at the 6m telescope (BTA) of SAO RAS, with the MPFS spectrograph and the scanning Fabry-Perot Interferometer. NGC 2681 was also observed with long-slit spectrograph of the BTA. Optical and NIR images were obtained at the BTA and at the 2.1m telescope (OAN, Mexico). High-resolution images were retrieved from the HST data archive. Morphological and kinematic features of all 13 sample objects are described in detail. Attention is focused on the interpretation of observed non-circular motions of gas and stars in circumnuclear (one kiloparsec-scale) regions. We have shown first of all that these motions are caused by a gravitational potential of large-scale bar. NGC 3368 and NGC 3786 have nuclear bars only, their isophotal twist on the larger radii being connected with the bright spiral arms. Three cases of inner polar disks in our sample (NGC 2681, NGC 3368 and NGC 5850) are considered. We found ionized-gas counter-rotation in the central kiloparsec of the lenticular galaxy NGC 3945. Seven galaxies (NGC 470, NGC 2273, NGC 2681, NGC 3945, NGC 5566, NGC 5905, and NGC 6951) have inner mini-disks nested in large-scale bars. The morphological and kinematical features in the sample galaxies can be explained beyond the secondary bar hypothesis. Thus we suggest that a dynamically independent secondary bar is a much more rare phenomenon than it follows from isophotal analysis of the images only.

Key words. Galaxies: kinematics and dynamics { Galaxies: spiral { Techniques: spectroscopic

1. Introduction

More than a quarter of a century ago de Vaucouleurs (1975) found that an inner bar-like structure was nested in the large-scale bar in the optical image of NGC 1291. The first systematic observational study of this phenomenon was made by Buta & Crocker (1993), who published a list of 13 galaxies, where the secondary (inner) bar was arbi-

trarily oriented with respect to the primary (outer) one. In the following years the isophotal analysis technique had allowed to detect secondary bars in optical (Wozniak et al., 1995; Erwin & Sparke, 1999; Erwin & Sparke, 2003) and NIR images of barred galaxies (Friedli et al., 1996; Jungwiert et al., 1997; Laine et al., 2002). Up to now, we have found 71 candidate double-barred galaxies in the literature (see references in Moiseev, 2001b). A new revised catalog of 67 barred galaxies including 50 double-barred ones is presented by Erwin (2003). Although various theoretical works exist, the secondary bar dynamics is still far from being well understood. Shlosman et al. (1989) have shown that an additional circumnuclear bar may be formed as a result of instabilities of the gaseous ring in the Inner Lindblad Resonance (ILR) within a large-scale bar. Heller et al. (2001) present a detailed simulation of this process, which, unfortunately, results in appearance of an elliptical gaseous ring instead of the "real" stellar-gaseous bar. Maciejewski & Sparke (2000) found some families of closed orbital loops, able to support both bars. Similar independently rotating structures sometimes appear in

Send offprint requests to: A. V. Moiseev e-mail: moisav@sao.ru

[?] Based on observations carried out at the 6m telescope of the Special Astrophysical Observatory of the Russian Academy of Sciences, operated under the financial support of the Science Department of Russia (registration number 01-43), at the 2.1m telescope of the Observatorio Astronómico Nacional, San Pedro Martir, Mexico, and from the data archive of the NASA/ESA Hubble Space Telescope at the Space Telescope Science Institute. STScI is operated by the association of Universities for Research in Astronomy, Inc. under NASA contract NAS 5-26555.

^{??} Guest User, Canadian Astronomy Data Center, which is operated by the Herzberg Institute of Astrophysics, National Research Council of Canada.

stellar-gaseous simulations of galactic disks (Pfenninger & Norman, 1990; Friedli & Martinet, 1993). New hydrodynamical simulations of the gas behavior in double bars, with an analysis of the problems arising during modeling and interpretations of the double-barred structures are presented by Maciejewski et al. (2002) and Shlosman & Heller (2002).

Various observational data indicate that we are seeing probably a new structural feature of barred galaxies in the case of double bars. However, the majority of observational results have been based on photometric measurements only, when an elongated elliptical structure appears inside the large-scale bar. Moreover, using the isophotal analysis formalism (Wozniak et al., 1995) has allowed even "triple bars" (Friedli et al., 1996; Jungwiert et al., 1997; Erwin & Sparke, 1999) without any arguments about the dynamical behaviors of such complex stellar systems. At the same time, the structures seen in direct images can be explained in a less exotic manner, without using the hypothesis of double or triple bars. A lot of structural features would be able to create an illusion of a secondary bar (Friedli et al., 1996; Moiseev, 2001b; Petitpas & Wilson, 2002), such as for example, an oblate bulge, a complex distributions of dust and star formation regions in the circumnuclear region, or elliptical rings at the ILRs of a primary bar (Shaw et al., 1993). Therefore new observational data is required to test our understanding of the secondary bar phenomenon.

Kinematic data (the stars and gas line of sight velocities and velocity dispersion) over circumnuclear regions of barred galaxies is of crucial importance for this kind of studies. Recently, Emselfem et al. (2001a) have studied the kinematics of double-barred galaxies candidates and make a conclusion on dynamical decoupling of the circumnuclear regions in NGC 1097, NGC 1808 and NGC 5728. This conclusion is based on the fact that peaks of the relative line-of-sight velocities and stellar velocity dispersion drops are seen in the circumnuclear regions from long-slit cross-sections. Wozniak (2000) have supposed that "counter-rotation" of stars, observed in the nuclear region of NGC 5728, may be associated with secondary bar influence on stellar kinematics. All these features observed in the one-dimensional data may be explained without using the hypothesis of secondary bars. This fact may be related to the specific mass distributions in the inner kiloparsec and to non-circular motions of stars and gas within the primary bar only (x_2 -families of stellar orbits lead to the "counter-rotation" properties). Also Wozniak et al. (2003) in their self-consistent N-body simulations have shown that the velocity dispersion drops observed by Emselfem et al. (2001a) can be independent on the presence of a secondary bar and are reproduced in the model a single-barred galaxy.

Since the motions of stars and gas inside the bar region are strongly non-circular, and such objects are non-axisymmetric by definition, the panoramic (also named 2D, 3D or integral-field) spectroscopy should give us a more detailed information on circumnuclear kinematics

in relation to "classical" (long-slit) spectroscopy. The integral-field spectroscopy makes it possible to map two-dimensional fields of line of sight velocities and velocity dispersion. Therefore, during 2000–2002 we have carried out a series of observational programs on 2D-kinematics and morphology of double-barred galaxies candidates. The main goal was to find an answer to the question "Are the secondary bars dynamically decoupled systems?"

This problem is complicated and ambiguous because of the lack of theoretical works, where the "observed" velocity fields in the double-barred galaxies had been modeled. It is important to collect a full sample of candidate double-barred with observable 2D-kinematics of stars and gas. These observations must be used to search for common dynamical (kinematic) features in these kinds of galaxies. Recently, Shlosman, & Heller (2002) have written: "Clearly, the most promising method in detecting the nuclear bars is two-dimensional spectroscopy of the central kiloparsec, which can reveal the underlying kinematics".

Our observational program has been finished in 2002. Independently a similar observations were started at the 3.6m CFHT by using the integral-field spectrographs OASIS and TIGER. Recently, the velocity fields of stars and ionized gas in some double-barred candidates is presented by Emselfem & Friedli (2000), Emselfem et al. (2001b) and Emselfem (2002). The velocity fields of the molecular gas were also investigated in double-barred candidates NGC 2273 and NGC 5728 (Petitpas & Wilson, 2002) and NGC 4303 (Schinnerer et al., 2002).

In this work, we present the observational data (integral-field spectroscopy and NIR/optical surface photometry) for 13 galaxies and discuss the problem of central regions dynamical decoupling. The paper is structured as follows. In Sect. 2 we describe the observations and data reduction technique. The methods of analysis of the velocity fields and surface brightness distributions are considered in Sect. 3. In Sect. 4 we present the notes for individual observed galaxies and discuss their common properties in Sect. 5; a small conclusion is drawn in Sect. 6.

2. Observations and data reduction

We have compiled our sample from Moiseev (2001b) by applying the following restrictions: $\alpha > 0$, and the size of major axis of the probable secondary bar being smaller than or equal to the MPFS field-of-view ($16'' \times 15''$). We have obtained full observational data for 13 galaxies, that is for about one third of the candidates on the Northern sky.

2.1. Integral-field spectroscopy with the MPFS

Circumnuclear regions of all the galaxies were observed at the 6m telescope of the Special Astrophysical Observatory, Russian Academy of Sciences (SAO RAS) with the Multipupil Integral Fiber Spectrograph (MPFS, Afanasiev et al., 2001). A description of the spectrograph is also available through the Internet at SAO WEB-

page <http://www.sao.ru/hq/lsvfo/devices.html>. The spectrograph takes simultaneous spectra from 240 spatial elements (constructed in the form of square lenses) that form an array of 16 × 15 elements on the sky. The field of view is 16⁰⁰ × 15⁰⁰, and the angular size is 1⁰⁰/element.

Three galaxies, NGC 2273, NGC 3368, and NGC 3945 were observed in two different positions of the multi-lens array on the sky, with each frame containing a galactic nucleus. After preliminary data reduction, the "data cubes" were combined. The resulting field of view was 16⁰⁰ × 18⁰⁰ for NGC 2273, 18⁰⁰ × 18⁰⁰ for NGC 3368 and 23⁰⁰ × 23⁰⁰ for NGC 3945. Together with target spectra, we took a night-sky spectrum from an area located at 4⁹⁵ from the center of the field of view. The detector was a TK 1024 1024 1024 pixels CCD array. The spectrograph reciprocal dispersion was 1:35 Å/pixel and the spectral resolution was about 4 Å. The log of M PFS observations is given in Table 1. It contains the names of galaxies, dates of the observations, the total exposures T_{exp} , the spectral range and the seeing quality during the exposures.

We reduced the observations by using the software developed at the SAO RAS by V.L. Afanasiev and running in the IDL environment. The primary reduction included bias subtraction, flat-fielding, cosmic-ray hits removal, extraction of individual spectra from the CCD frames, and their wavelength calibration using a spectrum of a He-Ne-Ar lamp. Subsequently, we subtracted the night-sky spectrum from the galaxy spectra. The spectra of spectrophotometric standard stars were used to convert the fluxes into absolute energies.

The reduced spectra were represented as "data cubes": each spatial element of the two-dimensional field has an individual 1024-channel spectrum. We constructed the maps of line intensity and light-of-sight velocity fields in the H α , [O III] 4959; 5007 Å and/or [N II] 6548; 6583 Å lines by means of the Gaussian fitting of the emission line profiles. A double-Gaussians model was used for doublets separation. The absolute accuracy of the velocity determination, evaluated from the air-glow lines wavelengths, was about 10–15 km s⁻¹. For the continuum map construction we summed the fluxes in the spectral ranges free of the emission lines (5600–5800 Å for "green" and 6350–6450 Å for "red" spectra).

The line of sight velocity and velocity dispersion fields for stellar component were constructed by means of a cross-correlation technique, modified for the M PFS data (Moiseev, 2001a). The used spectral region included some stellar absorption features; Mg I 5175 Å, Fe I 5229 Å, Fe I Ca I 5270 Å, and Na I 5893 Å among others. The spectra of G 8-K 3 giant stars and the twilight sky, observed during the same nights, were obtained as velocity templates. In order to take into account the variations of the instrumental contour (see Moiseev, 2001a), during the template's observations, the images of stars were out-of-focus to fill the M PFS field-of-view. The accuracy were of 10 km s⁻¹, and 10–20 km s⁻¹ respectively for the velocity and velocity dispersion determinations (the errors are dependent on the cross-correlation peak amplitudes).

2.2. Observations with the Fabry-Perot Interferometer

Six galaxies with bright emission lines were observed at the 6m telescope with the scanning Fabry-Perot Interferometer (IFP). The Queensgate interferometer ET-50 was used in 235 interference order (for H α line). The free spectral range between neighboring orders (interfringe) was about 28 Å (1270 km s⁻¹). For preliminary monochromatization, a set of narrow-band filters, with a FWHM = 12–18 Å and centered on the spectral region containing redshifted H α or [N II] 6583 Å emission lines were used. During the observations we consequently take 32 interferometric images of an object through the interferometer with different gaps between IFP plates. The spectral channels have a width of 0.9 Å (40 km s⁻¹), the spectral resolution (the width of instrumental contours) was FWHM = 2.5 Å (110 km s⁻¹). The detector was a CCD TK 1024 (1024 × 1024 pixels). The CCD was operated with 2 × 2 binning for reading-out time economy. Therefore each spectral channel has a 512 × 512 pixel format.

In February and March, 2000, the IFP was installed into the parallel beam, inside the focal reducer (Dodonov et al., 1995; Moiseev, 2000). The resulting focal ratio at the prime focus of 6m telescope was F=2.4, with a field-of-view of 5⁹⁸ and a scale of 0:68⁰⁰=px.

In September and November 2000, the observations were carried out with the new multi-mode focal reducer SCORPIO. A brief description of this device is given in Internet (<http://www.sao.ru/hq/moisav/scorpio/scorpio.html>), also the IFP mode in SCORPIO is described by Moiseev (2002a). With this configuration, the focal ratio was F=2.9, with a field-of-view of 4⁹⁸ and a scale of 0:56⁰⁰=px. The log of the IFP observations is presented in Table 2.

To reduce the interferometric observations we used a custom development software (Moiseev, 2002a), running in the IDL environment. After primary reduction (bias, flat-fielding etc.), removing the night-sky emission lines and converting to the wavelength scale, the data were presented as "data cubes". In such cube, to every pixel of the 512 × 512 field, a 32-channel spectrum is attached. The "data cubes" were smoothed by Gaussians with a width, in the spectra domain, of FWHM = 1.5 channel, and in the spatial (sky-plane) domain of FWHM = 2–3 pixels under the ADHOC package¹. The ionized gas velocity fields, and the emission lines images were mapped by means of a Gaussian fitting of the emission line profiles. Moreover, we created the images of the galaxies in the "red" continuum nearby to the emission lines.

2.3. NIR photometry at 2.1m telescope

The NIR surface photometry of the sample galaxies was carried out with the CAMILA camera (Cruz-Gonzalez

¹ ADHOC software has been written by J. Boulesteix (Observatoire de Marseille). See <http://www-obs.cnrs-mrs.fr/ADHOC/adhoc.html>

Table 1. Log of MPFS observations.

Name	Date	T _{exp} , sec	λ , Å	Seeing	
NGC 470	01/09/2000	4	1200 4820	6190 2.8 ⁰⁰	
NGC 2273	01/12/2000	6	1200 4770	6140 2.5 ⁰⁰	
NGC 2681	30/03/2000	4	1200 4840	6210 2.0 ⁰⁰	
	09/03/2002	3	900 5800	7170 1.7 ⁰⁰	
NGC 2950	27/03/2000	3	1200 4840	6210 2.0 ⁰⁰	
NGC 3368	27/03/2000	7	1200 4840	6210 2.5 ⁰⁰	
NGC 3786	27/03/2000	4	1200 4840	6210 2.5 ⁰⁰	
NGC 3945	01/12/2000	6	1200 4770	6140 2.5 ⁰⁰	
	13/05/2002	2	1200 4700	6070 1.5 ⁰⁰	
	13/05/2002	2	3	1200 5900	7270 1.5 ⁰⁰
NGC 4736	11/05/2000	3	1200 4840	6210 1.8 ⁰⁰	
NGC 5566	10/05/2000	3	1200 4840	6210 2.3 ⁰⁰	
NGC 5850	13/08/2001	3	1200 5710	7080 2.7 ⁰⁰	
	13/05/2002	3	1200 4700	6070 1.2 ⁰⁰	
NGC 5905	30/03/2000	8	1200 4840	6210 2.0 ⁰⁰	
NGC 6951	03/09/2000	5	1200 4840	6210 2.2 ⁰⁰	
NGC 7743	02/09/2000	3	1200 4840	6210 2.0 ⁰⁰	

Table 2. Log of IFP observations.

Name	Date	T _{exp} , sec	Line	Seeing
NGC 470	02/11/2000	32	200 H	2.1 ⁰⁰
NGC 2273	03/11/2000	32	200 H	2.0 ⁰⁰
NGC 3368	28/02/2000	32	150 H	2.7 ⁰⁰
	28/02/2000	32	200 [N II]	3.5 ⁰⁰
NGC 3945	03/11/2000	32	190 [N II]	2.0 ⁰⁰
NGC 4736	02/03/2000	32	150 H	2.7 ⁰⁰
	02/03/2000	32	180 [N II]	3.5 ⁰⁰
NGC 6951	23/09/2000	32	120 H	2.5
	23/09/2000	32	120 [N II]	2.5 ⁰⁰

et al., 1994) in the JHK⁰ bands, at the 2.1m telescope of the Observatorio Astronómico Nacional, San Pedro Martir, México. CAM ILA is equipped with a NICMOS3 256 × 256 pixels detector. Observations were carried out with two telescope focuses, under different focal ratios. In the F=13.5 mode the field-of-view was 1.3 and the pixel size 0.30. The F=4.5 mode provided a field-of-view of 3.6 with a scale of 0.85=px. The log of the NIR observations is given in Table 3.

Each observation consisted of a sequence of object and sky exposures, with the integration time of an individual exposure limited by the background level, which was kept well below the non-linear regime of the control electronics. The nearby sky frames were taken with the same exposure times and at adjacent positions to the object, through an observing sequence that alternates the object and sky frames.

The routines under Image Reduction and Analysis Facility (IRAF) were used in the reduction and analysis of all the data. The image processing involved subtraction of sky frames, division by flat frames, registration of the images to a common coordinate system and stacking

Table 3. Log of CAM ILA observations.

Name	Date	Mode	Filters	Seeing
NGC 2273	09/03/2001	(F=4.5)	J, H, K ⁰	3.5 ⁰⁰
NGC 2681	09/03/2001	(F=4.5)	J, H, K ⁰	2.8 ⁰⁰
	18/03/2000	(F=13.5)	J, H, K ⁰	1.5 ⁰⁰
NGC 2950	12/03/2001	(F=4.5)	J, H	3.0 ⁰⁰
	18/03/2000	(F=13.5)	J, H, K ⁰	1.5 ⁰⁰
NGC 3368	12/03/2001	(F=4.5)	J, H	2.2 ⁰⁰
	18/03/2000	(F=13.5)	J, H, K ⁰	1.5 ⁰⁰
NGC 3786	19/03/2000	(F=13.5)	J, H	1.5 ⁰⁰
NGC 3945	09/03/2001	(F=4.5)	J, H	4.0 ⁰⁰
	18/03/2000	(F=13.5)	J, H, K ⁰	1.5 ⁰⁰
NGC 4736	20/03/2000	(F=4.5)	J, H, K ⁰	1.5 ⁰⁰
NGC 5566	18/03/2000	(F=13.5)	J, H, K ⁰	1.5 ⁰⁰
	12/03/2001	(F=4.5)	J, H	1.5 ⁰⁰
NGC 5850	18/03/2000	(F=13.5)	J, H, K ⁰	1.5 ⁰⁰
NGC 5905	19/03/2000	(F=13.5)	J, H	2.5 ⁰⁰

all the images in a filter. Bias subtraction was carried out during the data acquisition. Some of the images had a horizontal band at the joints of the individual quadrants of the NICMOS3 array detector. We eliminated this feature by subtracting a 255 × 1 pixels median smoothed image from the original images.

2.4. Direct imaging at the 6m telescope

Optical direct imaging observations of some galaxies were carried out with the focal reducer SCORPIO (Sec. 2.2) at the 6m telescope. The detector (CCD TK 1024, 1024 × 1024 pixels) provided a field of view of 4.8 with a pixel scale of 0.28. The log of observations is presented in Table 4. We used 3 filters: V (Johnson), R_c (Cousins) and a medium-band red filter (SED 755) for the continuum imaging of the objects (without any pollution from the object's emission lines). The SED 755 filter has a width of FWHM = 220 Å and is centered at 7560 Å. The data reduction included bias and flat-field corrections, and cosmic hits removing.

2.5. Hubble Space Telescope data

We also used the high-resolution images of the sample galaxies available from the HST Archive. The HST images were obtained with the optical WFC2 and the infrared NICMOS cameras. WFC2 has an image scale of 0.1⁰⁰=px and a field-of-view of 2.7 and 0.045=px for the Planetary Camera (PC), with a field-of-view of 36⁰⁰. The NICMOS detector includes three chips. Its pixel scale and field-of-view are 0.043 and 11⁰⁰ for NIC 1, 0.075 and 19⁰⁰ for NIC 2, and 0.2 and 51⁰⁰ for NIC 3. The information about the archival images is given in Tab 5. Here ID is an archive identification of the observational program.

Table 4. Log of direct imaging observations at the 6m telescope

Name	Date	Filters	Seeing
NGC 470	03/11/2000	V, R _c , SED 755	1.4 ⁰⁰
NGC 2273	03/11/2000	V, R _c	1.0 ⁰⁰
NGC 2681	25/10/2000	V	1.0 ⁰⁰
NGC 2950	04/11/2000	V, R _c	1.5 ⁰⁰
NGC 3945	03/11/2000	V, R _c	1.0 ⁰⁰
NGC 6951	04/11/2000	V, R _c , SED 755	1.2 ⁰⁰
NGC 7743	03/11/2000	V, R _c , SED 755	1.5 ⁰⁰

Table 5. HST high resolution direct images

Name	Date	Camera	Filters	ID
NGC 2273	05/02/1997	WFPC2	F791W	6419
	03/04/1998	NIC2	F160W	7172
	03/04/1998	NIC3	F164N, F166N	7172
NGC 2681	07/06/1998	NIC3	F187N, F160W	7919
	03/09/2000	WFPC2	F300W	8632
NGC 2950	26/01/1999	WFPC2	F450W, F555W, F814W	6633
NGC 3368	04/05/1998	NIC2	F160W	7331
	08/05/1998	NIC2	F110W	7331
	12/12/2000	WFPC2	F814W	8602
NGC 3786	30/03/1995	WFPC2	F606W	5479
	29/04/1998	NIC1	F110W, F160W	7867
NGC 3945	11/05/1997	WFPC2	F450W, F555W, F814W	6633
NGC 4736	02/07/2001	WFPC2	F814W	9042
NGC 5566	04/04/1999	WFPC2	F606W	6359
NGC 6951	30/10/2000	WFPC2	F814W	8602
	18/11/2000	WFPC2	F606W	8597
NGC 7743	30/05/1994	WFPC2	F547M	5419
	11/10/1994	WFPC2	F606W	5479
	16/09/1997	NIC2	F160W	7330

2.6. Long-slit observations of NGC 2681

When all the data were reduced and analysed we have seen that the photometric and MPFS data were not enough for understanding the outer morphology in NGC 2681; first of all, the disk's PA was very uncertain (Sect. 4.4). For this goal additional observations of this galaxy were performed in April-May of 2003 at the 6m telescope with the SCORPIO focal reducer in a long-slit mode. The detector was the EEV 42-40 2048 × 2048 pixels CCD array. The spectrograph reciprocal dispersion was 0:85Å/pixel, and the spectral resolution was about 6Å. The slit of 1.2⁰⁰ × 5.3⁰⁰ was centered onto the nucleus under three fixed orientations near possible minor (PA = 30° and 61°) and major (PA = 121°) axes. The log of observations is given in Table 6. Though the seeing condition was 2.5⁰⁰–3.5⁰⁰ on April 7, this fact isn't important for study of the outer regions' kinematics. The primary reduction included bias subtraction, flat-fielding, cosmic-ray hits removal. Then the individual spectra were sampled along the slit with

Table 6. Log of long-slit observations

Name	Date	PA	T _{exp, sec}	Seeing
NGC 2681	07/04/2003	30	4 600	2.6 ⁰⁰
NGC 2681	07/04/2003	61	3 900	3.5 ⁰⁰
NGC 2681	01/05/2003	121	3 1200	1.5 ⁰⁰

the bin of 0.6⁰⁰ at the distances $r < 10''$ from the center and with the bin of 2.5⁰⁰ at the larger distances. The spectrum of H e-N e-A r lamp was used for wavelength calibration. The line-of-sight velocity distributions along the slit were constructed by means of a cross-correlation technique. The spectra of the K 0 III stars observed in the same nights were used as velocity templates. The errors of the velocity measurements are from 10 km s⁻¹ in the galactic center till 20–30 km s⁻¹ at the distances of $r = 40–45''$.

3. A analysis of the velocity fields and photometric data

The isophote analysis of the images was performed with the FITELL program written by V.V. Vlasjuk (SAO RAS) which use the well-known algorithm of Bender & Moellenho (1987). It yields a surface brightness value (I) and the orientation parameters of elliptical isophotes: position angle PA, and ellipticity $\epsilon = 1 - b/a$, where a and b are the semi-major and semi-minor axis of ellipses respectively.

The velocity fields were analyzed by means of the "tilted-ring" method (Begeman, 1989), with fixed systemic velocity and position of the center as described by Moiseev & Mustsevoi (2000). Here we briefly describe the method. The velocity field is broken down into the elliptical rings, with a 1–1.5⁰⁰ width aligned with the line of nodes direction. Using the 2D minimization of the deviations of the observational points from the model, we calculate all 6 parameters, characterizing the pure circular rotation at the given radius R in the galactic plane. They are: the coordinates of the rotation center on the sky plane (x_0, y_0), the systemic velocity V_{sys} , the position angle of the major axis PA_{dyn} (dynamical position angle), the galactic plane inclination to the line of sight i , and the mean rotation velocity V_{rot} . However, since all galaxies contain large-scale bars in the inner regions and spiral arms in the outer ones, the "circular" velocity fields in the observed galaxies must be distorted by non-circular motions. The non-circular motions result in the systematic errors when determining the disk orientation parameters (see Appendix in Lyakhovich et al., 1997; Barnes & Sellwood, 2003; Fridman et al., 2003).

In such a situation it is convenient to fix some model parameters. A good first approach is to assume $x_0; y_0; V_{sys};$ and $i = \text{const}$, having only two free parameters for fitting in each ring: V_{rot} and PA_{dyn} . The PA_{dyn} deviations from the line of nodes of the whole disk (PA_0) is used to characterize the type of non-circular mo-

tions (oval distortion, polar disk, etc.). In the case of the motions of gas clouds in a bar potential, the observable PA_{dyn} ceases to be aligned with the disk's line of nodes (Chevalier & Furenlid, 1978, Moiseev & Mustsevoi, 2000). A turn of the "dynamical axis" must occur in the opposite direction, with respect to position angle of the inner isophotes, or to "photometric axis" (Moiseev & Mustsevoi, 2000). The same effects should be also observed in the velocity field of stars, as it is shown by numerical simulations (Miller & Smith, 1979; Vauterin & Dejonghe, 1997), and by analytical calculations of the star motions under the effects of a triaxial gravitational potential (Monnet et al., 1992). On the other hands, in the case of a pure circular rotation in a warped (polar, inclined) inner disk, the dynamical axis must follow the photometric one.

In determining the set of optimal galactic disk orientation parameters we are faced with some problems. For the systemic velocity V_{sys} we took its mean value over all radii. As the first approach, for the center position $x_0; y_0$ we took the coordinates of the symmetry center of a velocity field. If this "dynamical center" is at a distance less than 1.5^{00} from the center of the inner isophotes of the continuum image, then the photometric center is accepted as the ultimate center's position. In NGC 470 (Sect. 4.2), the difference between the positions of the dynamical and photometric centers exceeded the error of its measurement (the case of alopsided galaxy). For this galaxy we adopted the dynamical center as the center of rotation.

The main problem is to accurately calculate the values of the line of nodes position angle (PA_0) and the inclination (i). To use the averaged parameters of the outer isophotes is not always correct for this goal, because outer parts of the spiral structure distort these isophotes in galaxies possessing a well-developed spiral arms. It is also not evident the choice of radius range, where the average values of PA and i are calculated. In addition, some galaxies (NGC 3368, NGC 3945) have ring-like structures at large distances from the center. If a ring has a resonant origin, then it could be elliptical in the galactic plane (Buta, 1996) with uncertain ellipticity for an observer. Finally, the errors in flat-fielding and background-removing procedures (mainly for JHK⁰ images) also distort the shape of the low-brightness isophotes of the outer regions of galaxies. Therefore, we used the "spiral criterion", proposed by Fridman et al. (2003), for PA_0 and i determinations for the main part of our sample. This method is based on the applying of Fourier-series expansion to the surface brightness distribution in the galactic plane $I(R; \theta)$, where R is the radial distance, and θ the azimuthal angle:

$$I(R; \theta) = A_0(R) + \sum_{m=1}^N A_m(R) \cos(m\theta + \phi_m(R))$$

A_m , and ϕ_m are the amplitude and phase of the m -th harmonic, and $N = 8$ to 12 is the maximum number of the terms. If the m -armed spiral structure appears on the image, then the line of maximum of the harmonic number m should be also spiral. Clearly, in the bar region the

Table 7. Parameters of disk orientation

Name	$PA_0, (^\circ)$	$i, (^\circ)$
NGC 470	157	1 55
NGC 2273	58	2 50
NGC 2681	148	5 25
NGC 2950	119	1 50
NGC 3368	135	5 48
NGC 3786	247	5 61
NGC 3945	157	2 52
NGC 4736	298	6 31 ¹
NGC 5566	210	3 64
NGC 5850	335	10 37
NGC 5905	130 ²	40 ²
NGC 6951	140	6 41
NGC 7743	270	5 40

¹ Mukler (1995)

² van Moorsel (1982)

line of maximum of harmonics, $m = 2$ must be straight and elongated along the position angle of the bar. It appears that the shape of the spiral, traced by the maximum of harmonics, is very sensitive to selection of parameters of orientation. It may be shown that, if for a two-armed galaxy the inclination i is underestimated, then the line of maximum $m = 2$ at large radii will be fixed near the line of nodes direction.

Similarly, if the adopted PA_0 differs from the "true" value, then the line of $m = 2$ maximum will be approximate to the direction of the "true" PA_0 in the outer part of the disk. Our experience shows that for moderate inclinations ($i = 30 - 70^\circ$), the parameters of disk orientations may be calculated with the uncertainty of few degrees. More detailed description of this method is given in Fridman et al. (2003). In the Table 7 we present the PA and i for our sample galaxies. During the search for the orientation parameters we tried to obtain some consistency between all three methods (isophotal analysis, analysis of the IFP velocity fields, and the "spiral criterion"). Nevertheless, the preference was given to the "spiral criterion". The details of the orientation results are considered in the discussion of individual galaxies.

4. The results

4.1. The Atlas

The images and the results of velocity fields analysis are presented in the Figs. 4-21. The left panels of Figs. 4-16 show the MPFS data. The top row contains the continuum images, the velocity field of the stars, and the map of the line of sight velocity dispersion (σ). The image in the brightest emission line of the ionized gas, the velocity field of this emission line and the map of ionized gas velocity dispersion (σ_{gas}) are given in the middle row. For the last map the width of the instrumental contour was taken into account. There are no ionized maps for NGC 2950, NGC 3368, NGC 4736, and NGC 5566, be-

cause emission lines are absent in the MPFS spectra of these galaxies. A gray scale is drawn, in km s^{-1} , for the velocity fields and for the velocity dispersion maps; while it is in $\text{erg s}^{-1} \text{cm}^{-2} = 2^{00}$ for the continuum and emission lines images, except for NGC 5850 in the [N II] emission lines, where the scale is in arbitrary counts. The cross marks the position of the adopted center of rotation in all MPFS maps. At the bottom we show the radial dependences of the rotation velocity V_{rot} and the position angle on the dynamical axis PA_{dyn} for the stellar and gaseous components. The dotted line marks the adopted position angle of the line of nodes (PA_0).

Examples of the images and isophotal analysis results are shown on the right panels of the Figs. 4-16. The left column contains ground-based images with the largest field-of-view, while the right column contains the same data for the circumnuclear regions ($r < 5 \cdot 20^{00}$), observed with the HST. The best-resolution ground-based images are presented for those galaxies where the HST data is absent. The logarithm-scaled images with the corresponding isophotes are presented in the top row of the panels. In the middle row we present the residual brightness distributions, after elliptical isophotes removed from the images. In this case, the gray scale is linear. The thick dotted line shows the maximum of $m = 2$ harmonic for the surface brightness, overlapped onto the ground-based images. At the bottom, we plot the parameters of the isophotes: PA and ellipticity versus major semi-axis. The scatter of measurements, through the different filters, gives us an information about the errors of elliptical model. The horizontal dotted line corresponds to the PA_0 value, and the vertical dotted line (in the left plot) marks the radial range, which is zoomed at the right plots.

The results of the IFP observations are shown in the Figs. 17-21, which include the continuum and H α and [N II] emission line images. A square-root gray-scale is used. The cross marks the dynamical center. Also shown is the velocity field with isovegetics. The thick black contour corresponds to the systemic velocity, while the thin contours indicate line of sight velocities in steps of 50 km s^{-1} . And the last plot shows the rotation curve (V_{rot}) and the kinematic position angles (PA_{dyn}). Here the dotted line marks the PA_0 value. For NGC 3368, NGC 4736, and NGC 6951 we present data in the H α and [N II] emission lines.

It is necessary to make a short notice about the errors of the V_{rot} determination. The formal errors of the model usually are $1-5 \text{ km s}^{-1}$ because every elliptical ring for fitting contains from several tens up to hundreds points (the last for IFP velocity fields). Nevertheless, the rotation curve, determined in the frame of pure circular motions, will be affected by systemic errors on the order of the spread in the observational velocities around the average values of the given radius (Lyakhovich et al., 1997; Fridman et al., 2003). The error bars of $V_{\text{rot}}(r)$ in our Figures must be interpreted as the deviation of the line of sight velocities from the models of circular rotation in each ring; i.e. the mean value of non-circular velocities.

Therefore the "real" circular rotation curve should coincide with our curves within the errors which are given in the Figs. 17-21.

In the following subsections we will present the results for individual sample galaxies.

4.2. NGC 470

The adopted orientation parameters, $PA_0 = 149^\circ 3'$, $i = 51^\circ 4'$, have negligible differences from the measurements of Garcia-Gomez & Athanassoula (1991). However, the parameters from Table 7 allow us to obtain a more smooth well-ordered spirals of $m = 2$ harmonic maximum. In the circumnuclear region, PA of the SED 755 isophotes matches the NIR data of Friedli et al. (1996), but it deviates by more than 25° from the measurements in V and R_c bands. This fact can be related to the dust extinction, more significant in the optical bands. The deviations of the PA_{dyn} from the line of nodes at $r = 8 \cdot 20^{00}$ (from the IFP data, see Fig. 17) are explained by us as an effect of the large-scale (primary) bar on the ionized gas velocities. The turn of PA_{dyn} occurs in the opposite direction with respect to the inner isophotes PA (Fig. 4), in agreement with existing models of the gas flowing within the bars (see Sect. 3). Also the MPFS data reveals that the dynamical axis, for the stellar component, turns in the same direction as the gaseous (in H α) one at $r > 5^{00}$.

The center of rotation (dynamical center) of the MPFS velocity fields of stars and gas is shifted by 4^{00} (0.6 kpc), in the NW direction, from the photometric center. The discrepancy between the positions of both centers is considerably larger than the measurement errors or a possible effect of dust absorption. The difference in the locations of the centers is also observed in the large-scale H α velocity field, that confirms the result of Emmellen (2002). Such discrepancy in the photometric and dynamical centers locations or between centers of the inner and outer isophotes (lopsided-structure) have been seen in numerous galaxies (Richter & Sancisi, 1994). The nature of the lopsidedness could be different at different radial scales, from the circumnuclear disk precessing around a supermassive black hole to development of a spiral azimuthal disturbance $m = 1$ mode in the large-scale stellar-gaseous disk (Junquera & Combes, 1996; Emmellen et al., 2001a; Emmellen, 2002).

Tumbul et al. (1997) have proved that NGC 474 shows signs of interaction with NGC 470. They also noted that both galaxies are perhaps embedded into a common HI-cloud. Hence, the excitation of the non-axisymmetric harmonics in NGC 470 may be caused by a tidal interaction with the companion.

An alternative explanation can also be proposed for the lopsided since the distorted region is relatively small and located inside the large-scale bar. It is possible to suppose an abnormal development of the non-axisymmetric harmonics in the surface brightness during the secular evolution of a barred galaxy. The shift between the isophotal

center and the dynamical center is observed in the central regions of some barred galaxies (Zasov & Khoperskov, 2002).

Wozniak et al. (1995) assumed that the isophotal turn at $r < 7''$ was connected with a secondary bar. However later Friedli et al. (1996) have explained this feature by a triaxial bulge in the primary bar. This explanation is problematic from our point of view, because the position angle of the inner isophotes (at the $r = 2.6''$) is close to the disk PA_0 value. And the amplitude of isophotal PA deviations from PA_0 decreases sharply when passing from short wavelengths (V) to longer ones (SED 755). Such behaviour of the isophotes can be explained by dust extinction. Also the apparent ellipticity of the inner isophotes $\epsilon = 0.3 - 0.45$ (Fig. 4) corresponds to the projection of a circular disk onto the sky plane (if problems with bulge and outer bar deprojection will be taken into account). In Sect. 5.3 we decompose surface brightness distribution in NGC 470 and prove this assumption. Thus we think that there is a circumnuclear disk within the large-scale bar (see Sect. 5.3 for additional arguments. In the H velocity field the turn of PA_{dyn} occurs in the same direction with respect to the PA of isophotes at $r < 5.7''$ (Fig. 17). Such dynamical feature is also in agreement with circular motions in the decoupled disk which may be slightly inclined to the galactic plane (Sec. 3). An asymmetrical $m = 1$ harmonic is developed in this disk, which also has a large concentration of the molecular CO (Sofie et al., 1993), as well as of the ionized hydrogen (see the H - image on Fig. 17). The decoupling of the central disk may be caused by its location at the ILR of the large-scale bar.

Vega Beltran et al., (2001) gave an estimation of the central velocity dispersion of stars; $\sigma = 56 - 31 \text{ km s}^{-1}$ from their long-slit observations of NGC 470. However, such a low value of σ is doubtful, as it is difficult to explain the fact that the rotation velocity of stars (from our MPFS data), in the central region, is smaller by 50 km s^{-1} than the gas velocity. Our measurements support a central velocity dispersion of $140 - 150 \text{ km s}^{-1}$, that looks more realistic and agrees with estimations of Heraudeau et al. (2001).

In the H velocity field, at distances of $r = 12 - 20''$ to the East from the center, we observe a region with the line of sight non-circular motions about $50 - 60 \text{ km s}^{-1}$. The profile of the H emission line has a complex multi-component structure. Clearly, two or more systems of the gaseous clouds, with different velocities along the line of sight, are present in this abnormal region. The non-circular motions apparently are not related to the bar dynamics because they are not symmetric relative to the galaxy center. We suppose an extragalactic gas cloud falling into the galactic disk. Similar shapes of the emission line profiles (at much larger distances from the center) were observed by us in NGC 1084 (Moiseev, 2000).

4.3. NGC 2273 (M 62)

Van Driel & Buta (1993) have described a complex morphology of this galaxy: a large-scale bar of $50''$ in diameter and two systems of the spiral arms ending at distances 1.1 and 1.6 from the center. The influence of this large-scale bar appears clearly in the IFP velocity field in the H emission line (Fig. 17): the dynamical axis deviates by more than 20° from the line of nodes PA_0 at radii $r = 3.45''$. The turn of PA_{dyn} occurs in the opposite direction with respect to PA of the isophotes at these distances (Fig. 5), in accordance with a common picture of gas flows in barred galaxies. The residual line of sight velocities along the minor axis have amplitudes of more than $50 - 80 \text{ km s}^{-1}$ (after pure circular model subtraction) at the radial distances of $10 - 13''$. The sign of residual velocities corresponds to the gas in motions² due the large scale bar. The PA_{dyn} radial variations in the H velocity field (from the MPFS observations) are in agreement with those in the H velocity field. Nevertheless, the amplitude of the H rotation curve (at $r = 1.6''$) is less by 50 km s^{-1} than the H rotation curve, and almost coincides with the rotation velocity of stars (Fig. 5). Apparently, the relatively weak H emission line is distorted by the broad absorption line from the underlying stellar spectrum.

The $[O III]$ velocity field significantly differs from the measurements in the Balmer lines. At $r < 3''$ the $[O III]$ line of sight velocities are constant, therefore the PA_{dyn} and V_{rot} are uncertain in this region. At the larger distances from the center the $[O III]$ gradient of the line of sight velocities is smaller than that of the hydrogen lines. We suggest that the existence of non-circular motions in forbidden lines is caused by the jet propagating outward from the Seyfert 2 nucleus. Ferruit et al. (2000) found a jet-like feature in the HST $[O III]$ -images and ionized maps ($[O III]=H$). It is seen, up to $2''$ to the east from the nucleus and coincides with the extended radiostructure. The spatial geometry of the gas motions around the jet cannot be restored from the MPFS data, most probably these motions are outside the galactic plane.

The stellar velocities do not reveal any non-circular motions in contrast with the gaseous velocities. The elliptical structure, elongated in E-W direction, appears in the stellar velocity dispersion map with a small drop of σ by $10 - 15 \text{ km s}^{-1}$ in the rotation center (Fig. 5).

Mulchaey et al. (1997) have discussed a secondary bar at $r < 8''$ from their NIR-photometry data. The high-resolution HST images showed that this "bar" breaks up into several elliptical arcs with radii of $r = 3 - 4''$ (see the residual brightness image in Fig. 5). Ferruit et al. (2000) described these features as a "pseudo-ring", and we suggest that it is a symmetric spiral twisted to the ring. This conclusion agrees with the Erwin & Sparke (2002, 2003) opinion. However Petitpas & Wilson (2002) returned toward a secondary bar assumption in the central kpc of

² We assume that spiral arms are trailing. Thus the NW-side of the galaxy is the nearest to an observer.

NGC 2273 based on their radio observation. We will discuss the molecular gas properties of the sample galaxies in Sect. 5.7. It will be shown that in the case of NGC 2273 the CO morphology agrees with the assumption of the inner stellar-gaseous disk embedded into the large-scale bar. The disk lies in the galactic plane and possesses a circum-nuclear spiral, as it is mentioned above.

4.4. NGC 2681

The sharp variations of the isophotal parameters (Fig. 6) reflect a complex morphological structure of the galaxy. Friedli et al. (1996) connected the radial turns of the isophotes with two bars, first proposed by Wozniak et al. (1995). Erwin & Sparke (1999) offered a model of the circum-nuclear structure of NGC 2681, consisting of three independent bars, with position angles of the major axes $PA_1 = 30^\circ$ ($20^\circ < r < 60^\circ$), $PA_2 = 75^\circ$ ($4^\circ < r < 20^\circ$) and $PA_3 = 20^\circ$ ($r < 4^\circ$). The smallest bar-like structure is seen in the HST NIRC2 images (Fig. 6).

However only isophotal analysis results are not enough to prove triple-barred structure because the photometry of the galaxy is a puzzle. We must note two items.

Firstly, this lenticular galaxy has no global spiral arms but its optical color maps (Wozniak et al., 1995; Erwin & Sparke, 1999) reveal short tightly wound spiral arms and numerous dust lanes in the region of "the middle bar" ($r = 10 - 20^\circ$). The majority of the dust lanes are located to the south from the nucleus and are extended along the spiral arms. These occulted mini-spirals also can be seen on our model-subtracted V-band image (Fig. 3) and unsharp masked R-band image by Erwin & Sparke (1999).

Secondly, the disk's position angle is uncertain from available imaging data. It varies from $PA_0 = 50^\circ$ (Friedli et al., 1996) till $130 - 140^\circ$ (Erwin & Sparke, 1999; 2003). The outer V-band isophotes (Fig. 6) have $PA = 110 - 120^\circ$. Also the PA_{dyn} in the circum-nuclear region (Fig. 6) differs from all these values. We tried to use a Fourier expansion method to search for disk orientation parameters and failed completely, because there are no symmetrical spirals in the galaxy.

The long-slit data helps to determine the disk orientation. Fig. 1 shows that the line-of-sight velocity gradient is absent along $PA = 61^\circ$. Hence this is direction of a minor axis (here we neglect possible non-circular motions in the bars). For more precise analysis we fitted velocities in all cross-sections by a model of pure circular rotation. The following values were found from a χ^2 -minimization: $PA_0 = 148.5^\circ$ and $i = 25.5^\circ$. These parameters differ systematically from the orientation of the outermost isophotes ($PA_0 = 140^\circ$, $i = 18^\circ$, Erwin & Sparke, 2003). It's possible that the outer disk contains a slightly elliptical ring.

The panoramic spectroscopy data (Fig. 6) show that stars at $r > 3 - 4^\circ$ exhibit a circular rotation where the value of PA_{dyn} matches the disk's line of nodes. But at $r < 2^\circ$ we observe strong changes of the stars dynamical axis

by $30 - 90^\circ$. The PA_{dyn} variations in the velocity field of the ionized gas are smaller but differ systematically from the stellar one by $10 - 15^\circ$ at $r > 3^\circ$. Also the symmetry center of the gas velocity field is shifted by 1.5° to the east from the continuum center, similarly to NGC 470. In addition, the sharp turn of the isoveLOCITIES is seen at $r < 2^\circ$ (80 pc). So, this region is dynamically decoupled concerning both the stars and the gas. At these distances, the value of PA_{dyn} of the stars is closer to the orientation of the HST inner isophotes ($PA = 25 - 35^\circ$). Such relation between the "photometric" and "kinematic" axes is a fact that does not point in the direction of the bar hypothesis, but of a disk-like kinematics. Thus an inclined (or polar) stellar-gaseous disk exists in the central few tens parsecs of NGC 2681. This disk is seen on HST images of the galaxy from UV (WFPC2) to NIR (NICMOS). Erwin & Sparke (1999) accepted this disk as a third (inner) bar on HST images. Unfortunately, the spatial sampling of the MPFS data is not sufficient for more certain conclusions on kinematics in this region (the seeing was $1.7''$).

Cappellari et al. (2001) have proved that NGC 2681 hosts a nuclear starburst of 10^9 yrs old. They considered a merger process with a small gaseous companion as the most probable trigger of the nuclear star formation. If the companion had a spin direction inclined to the galactic plane, then the remnants of the merged gas will be observed as a central inclined disk, and the non-orthogonal disk will be precess toward the galactic plane. However, a polar disk may be stable enough and rather long-living (Maboldi & Sparke, 1994). From this point of view the central structure of NGC 2681 is similar to that of galaxies with inner polar rings, as IC 1689 (Hagen-Thom & Reshetnikov, 1997) or UGC 5600 (Shalyapina et al., 2002). Nevertheless, the polar disk in NGC 2681 is smaller, of about 100 - 300 pc in diameter.

The merger hypothesis makes it possible to explain the spiral arms and dust lanes at $r < 20^\circ$, which have a shape differing from ordinary dust lanes in large-scale spiral arms. Also these occulted non-symmetrical spirals differ from symmetrical two-armed dust spirals which are usually observed near a shock front in barred galaxies. The H + [N II] ionized gas emission lines is also observed only at $r < 15^\circ$ (Wozniak et al., 1995). Thus, the stellar-gaseous disk, with spiral arms and perturbed dust layer³, is nested in the center of large scale-bar at $r < 15 - 20^\circ$ (600 - 900 pc). A strong asymmetry in the dust distribution may be associated with a possible warp of the gaseous-dust disk relative to the stellar one. We suggest, that all the features mentioned above (inner polar disk, abnormal shape of the spirals, and warp of dust layer) are caused by recent merging event.

We try to estimate positions of ILRs in NGC 2681. Figure 2 shows the polynomial approximation of the stel-

³ We suggest that the spiral in NGC 2681 has probably dust origin. Indeed, the spiral appears on the optical images and disappears on the J-band residual image (Fig. 6) as well as on NIR color maps (Friedli et al., 1996)

lar rotation curve. But the amplitude of circular velocities must be larger than these streaming velocities because velocity dispersion provides additional support against gravity. For asymmetric drift correction we used equation (2) from Aguerri et al. (2003) and their assumptions (the ratio of azimuthal to radial components of velocity dispersion $\sigma_{\phi} = \sigma_R = 1 - \frac{v_{\text{stream}}}{v_{\text{rot}}}$ (2), and disc's volume density decrease exponentially with radius). The drift correction was calculated for $\sigma_{\phi} = \sigma_R$ values 0.7 and 1.0, bracketing a possible range for early-type galaxies (Aguerri et al., 2003). The corrected circular velocities and the resonance curves shown on Figure 2 are truncated at the radius of $15''$ because the asymmetric drift approximation fails in the bulge-dominated region (see surface brightness profile in Fig. 3). For calculation of a bar's angular velocity Ω_{bar} we make the following assumptions: the maximal circular velocity is about $220 - 260 \text{ km s}^{-1}$; the bar size is $R_b = 60''$; the ratio radius can be 1 to $1.6 R_b$, this is the range observed for bars in lenticular galaxies (Aguerri et al., 2003). The probable range of the large-scale bar angular velocity, $\Omega_{\text{bar}} = 35 - 70 \text{ km s}^{-1} \text{ kpc}^{-1}$, is marked as gray rectangular in Fig. 2. This Figure also demonstrates that one or two ILRs could exist near the radius of $r = 20''$, if the Ω_{bar} is smaller than the probable ones. This distance coincides with the approximated size of the inner dust/gaseous disk described above. In this case the gas was accumulated by the bar's forces. Of course we must remember that the resonance curves are calculated for a symmetric potential without any bar perturbations. But we think that our evaluation of the ILR radius can be used as a zero approximation of the resonances' position.

In conclusion, we suggest the following interpretation to the NGC 2681 global morphology. The large-scale low-contrast bar dominates in the optical and NIR images at $r = 50 - 60''$ and has the ILRs at $r = 15 - 25''$. The decoupled gaseous disk is observed inside the resonance region. This inner disk is elliptical (non-circular) because the elongated orbits of stars change their major axis orientation at resonances (Lindblad, 1999). This elliptical disk was accepted by Erwin & Sparke (1999) as a secondary ("middle") bar. The recent dwarf companion merging leads the structure perturbation of the kiloparsec-size disk with inclined (polar) orbits in the central 100 pc.

4.5. NGC 2950

Our value of PA_0 differs slightly (by 10°) from measurements of Friedli et al. (1996). The radial dependences of the isophotal PA and ϵ , in all observed bands, coincide with those of Wozniak et al. (1995) and Friedli et al. (1996). The large-scale bar ($r = 30 - 40''$ in size) is seen over the distributions of the $m = 2$ Fourier harmonic and has a turn of isophotal PA accompanied by an ellipticity peak (Fig. 7).

Wozniak et al. (1995) and Friedli et al. (1996) explained the inner PA turn, and the peak, at $r < 6''$, as a secondary bar. Surprisingly, this "bar" does not distort

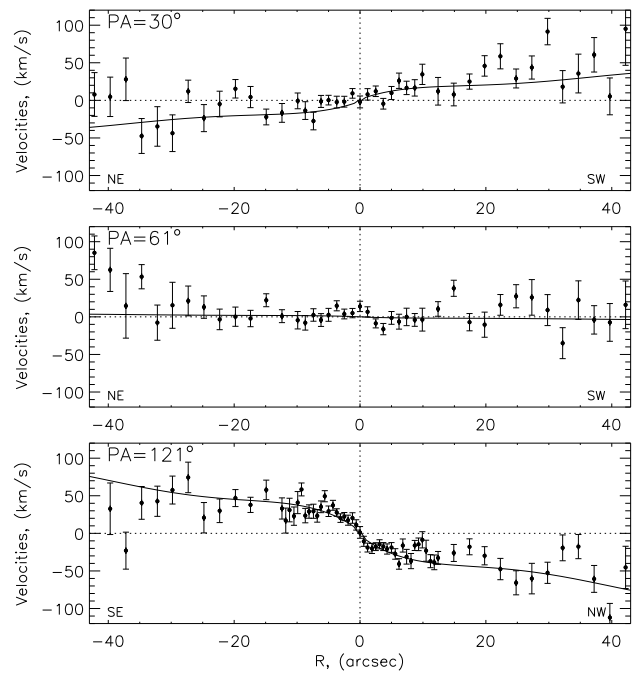


Fig. 1. NGC 2681: Stellar velocities measured along different position angles. Solid line marks the best-fitted model of the rotation curve

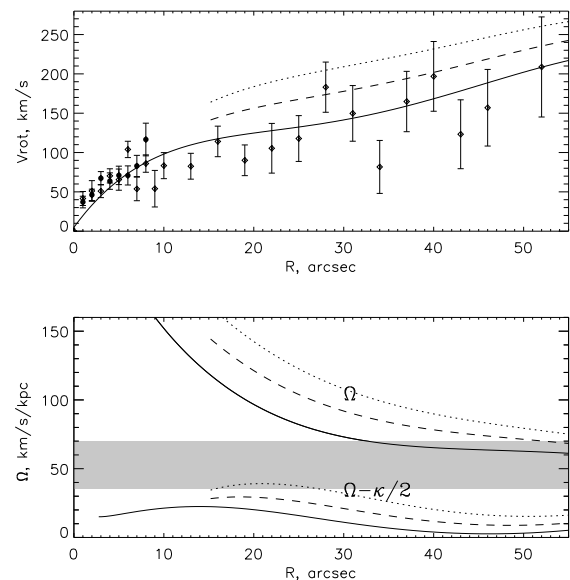


Fig. 2. top Rotation velocities of the stars in NGC 2681. Different symbols show MPFS (filled) and long-slit (open) data. The solid line is a polynomial fitting. The other lines mark the velocity streaming curves where asymmetric drift terms are taking in account with $\sigma_{\phi} = \sigma_R = 0.7$ (dotted) and 1.0 (dashed). bottom The angular velocities (Ω) and $\Omega = \kappa/2$ (where κ is an epicyclic frequency) curves calculated from the different models of the rotation curve. The thick rectangular shows the possible range of the bar's angular velocity.

the circular rotation of stars in the circum nuclear region. The PA_{dyn} of the stellar velocity field coincides with line of nodes position angle PA_0 .

We do not detect any non-circular motions in this velocity field despite the strong turn of isophotes at these radii. There are sharp elliptical structures decoupled in the stellar velocities dispersion map at $r = 1.5''$ (Fig. 7). It is extended along $PA = 150^\circ$, which is the direction of the major axis of the primary (external) bar.

4.6. NGC 3368 (Messier 96)

Sil'chenko et al. (2003) analyzed the results of panoramic spectroscopy of this galaxy including our observational data. However, that work is mostly focused on the stellar population properties. We will shortly describe the main properties of the inner kinematics of this galaxy which is a member of the Leo I group.

Observations with the scanning IFP allow us to map the large-scale velocity fields of the gas in two emission lines (Fig. 18). The H emission mostly concentrates in the star-forming ring, at distances of $50-70''$ from the center. Unfortunately, the stellar absorption features and the overlapping interference orders distort the emission line profiles in the H data-cube, over the whole central region of the galaxy. We cannot resolve this problem because the free spectral range of the IFP is rather small (28\AA). In contrast, the [N II] velocity field has been constructed over the full range of radii. The dynamical position angle of the outer gaseous disk, $PA_{\text{dyn}} = 170^\circ$, at $r = 30-200''$, differs strongly from the orientation of the line of nodes of the stellar disk, $PA_0 = 135^\circ$. The last value was calculated from the Fourier expansion of the NIR images ("spiral criterion", Sect. 3). Only for this value of PA_0 , the line of maximum $m = 2$ Fourier harmonic has a regular spiral shape and fits both spiral arms of the residual brightness distribution (Fig. 8). The isophotes, distorted by these spiral arms, were erroneously interpreted by Jungwiert et al. (1997) as a large-scale primary bar.

The orientation of the ionized gas disk $PA_{\text{dyn}} = 170-175^\circ$ has a good agreement with the outer part of the neutral hydrogen velocity field (Schneider, 1989) and with CO kinematics at $r < 15''$ (see Fig. 1 in Sakamoto et al., 1999). Thus, we suggest that gas (ionized/neutral) and stars in this galaxy rotate in different planes. All the gas in this galaxy, which is the brightest member of the western half of Leo group, has an external origin, in agreement with Schneider (1989). See Sil'chenko et al. (2003) for detailed arguments in favor of this possibility.

A good agreement exists between the measurements of the PA_{dyn} from two independent IFP velocity fields. Nevertheless, the [N II] rotation velocities are systematically lower, by 50 km s^{-1} , than the H ones. If the gaseous disk is inclined to the main galaxy plane, then shock-wave fronts can be developed at the cross-section of the global stellar and gaseous disks, since the gas strikes on the gravitational well. Thus, the low [N II] velocities

may be explained if the shock-excited gas, which is slowed down by collisions with the stellar disk and spiral arms (these intensify the contrast of the gravitation potential), emits mostly in the forbidden emission line. The discrepancy between velocities in the different emission lines is not an artificial instrumental effect. NGC 4736 was also observed, with the same technique in H and [N II] lines during the same observation run. And in the NGC 4736 data cubes the velocities in both emission lines are consistent with each other.

A large-scale ("primary") bar is absent in this galaxy, as it was mentioned above. However, a small-scale ($r = 5''$) nuclear mini-bar is present and extends along $PA = 120-125^\circ$. This bar provokes the turn of PA_{dyn} in the stellar velocity field by 25° , from the line of nodes in the opposite direction with respect to the PA turn of the inner isophotes (Fig. 8). The central asymmetry of the distribution is confirmed by long-slit spectroscopy of Vega Beltran et al. (2001).

The sharp turn of the isophotes, in the HST images inside $r = 2''$, may be associated with strong dust lanes. These lanes cross each the images near the nucleus and can be seen both in the optical and NIR images (Fig. 8). In Sil'chenko et al. (2003) we argue that a gaseous-dust mini-disk is located in the polar plane of the bar. Unfortunately, our MPFS and IFP data have a low angular resolution to study the polar disk kinematics.

4.7. NGC 3786 (M 74)

Our disk orientation parameters for this galaxy are in agreement with Afanasiev & Shapovalova (1981) results. Afanasiev et al. (1998) from their imaging data found two bars with semimajor axes of $7''$ and $25''$ in this Sy 1.8 galaxy. However, our Fourier-analysis of the optical and NIR images shows that the line of maximum of the $m = 2$ harmonic, at $r > 6-7''$, is wound to a regular spiral that coincide with the global two-armed spiral pattern of the galactic disk. This spiral appears also in the residual brightness maps (Fig. 9). Thus, the radial variations of PA of the inner isophotes, caused by the spiral arms, have led Afanasiev et al. (1998) to erroneous conclusion about large-scale bar in NGC 3786. The situation is the same as in the case of NGC 3368.

The PA_{dyn} of the velocity field of stars at $r < 6''$, differs from the line of nodes PA_0 by more than 10° . The deviations occur in the opposite direction relative to the central isophotes (Fig. 9). This indicates a dynamically decoupled central mini-bar of 2 kpc in diameter. The line of maximum of the $m = 2$ harmonic at $r < 5-6''$ has a constant azimuthal angle, a further confirmation of the mini-bar existence. The mini-bar was predicted by Afanasiev & Shapovalova (1981) from their long-slit data and confirmed photometrically by Afanasiev et al. (1998).

The ionized-gas velocity fields in the H and [O III] lines are different. More precisely, the orientations of PA_{dyn} in velocity field of the stars and gas in H coincide,

but the position angle, calculated from the [O III] velocity field of the gas, deviates from the stellar one. The deviations may be due to the presence of shock fronts at the bar edges, formed in the disk gas under the action of the bar gravitational well. The post-shock gas decelerates and emits in forbidden lines (Afanasyev & Shapovalova 1981, 1996). The rotation velocities in the [O III] line are smaller than those in the H α (Fig. 9). This feature may be also connected to breaking shock-excited gas at the bar edges.

The field of stellar velocity dispersion has a drop by 50 km s^{-1} in the center compared with that at $r = 3.4''$. This feature will be discussed in the Sect. 5.6.

4.8. NGC 3945

The radial variations of the isophotal parameters over all observed bands are in accordance with early observations of Friedli et al. (1996) and Erwin & Sparke (1999). The global spiral pattern is absent in this galaxy. The parameters of disk orientation were calculated under the assumption of a circular shape of the outer low-brightness ring ($r = 120\text{--}150''$). The values of PA_0 and i_0 agree (within the errors given in Table 7) with Erwin & Sparke (1999) and Erwin et al. (2003) results.

A large-scale bar extends along the galactic minor axis. Erwin & Sparke (1999) accepted that circumnuclear disk nests in the bar, because isophotal PA matches PA_0 at $r = 4.18''$. They favored also the existence of a secondary small bar embedded into the disk and found a low-contrast ring at $r = 7''$ as well. This ring is seen in our residual HST images (Fig. 10). The origin of this ring is discussed by Erwin et al. (2001).

The velocity field of stars in the circumnuclear disk shows a regular circular rotation (PA_{dyn} coincides with the PA_0). The fact of disk-like kinematics agrees with the conclusion by Erwin et al. (2003) that the inner disk is more luminous (and massive) than the bulge in this region. Also we must note that a possible secondary bar at $r < 3''$ suggested by Erwin & Sparke (1999) does not disturb the kinematics of the stars. The rotation curve agrees with early measurements of Bertola et al. (1995). A small difference in amplitude of the rotation curves, observed in 2000 and 2002, is probably due to a velocity gradient, smoothing by beaming effects, in observations with a worse seeing in 2000 (Table 1).

The velocity field of ionized gas is puzzle. Bertola et al. (1995) found the [O II] 3727Å line emission only in the very central region ($r < 3''$) and showed that the gas co-rotates with the stars. Nevertheless, our MPFS data contradicts Bertola et al. (1995) conclusions. First of all, we confidently detect the [N II] line emission up to a distance of $10''$ from the center. Secondly, inside the radius of $6''$ (about 0.5 kpc), the line of sight velocities of the gas are inverted with respect to the stellar velocities. Thus, a counter-rotating gaseous disk is located at $r < 5.6''$.

The direction of gas rotation becomes conformous with the stellar rotation at the larger distances from the

nucleus (see Fig. 10). The large-scale IFP velocity field (Fig. 19) confirms the fact of normal gas rotation at large radii, up to $140''$ (11 kpc). The variations of PA_{dyn} at $r = 5''\text{--}35''$ in the IFP velocity field are not real. This artifacts are caused by spectra overlapping of the strong stellar H α absorption and low-contrast [N II] emission lines in the central region. The small spectral range of the IFP observations does not allow us to separate absorption and emission lines. In contrast, at $r = 115''\text{--}140''$ the stellar continuum has a low contrast, while the [N II] lines are bright since they are emitted from some H II-regions in two spirals twisted to the outer ring.

4.9. NGC 4736 (Messier 94)

The outermost isophotes of our NIR images are limited to $r = 50''$, and we cannot calculate parameters of the outer disk orientation from these images. The application of the "tilted-ring" model to the [N II] velocity field at $r = 80\text{--}120''$ makes it possible to obtain the PA_0 value. The disk inclination is small and uncertain from velocity field analysis. Mulder (1995) found $i_0 = 31^\circ$ from the outer optical isophotes. We accept this value through our paper.

The velocity field of stars demonstrates a regular circular rotation with $PA_{\text{dyn}} = 300\text{--}305^\circ$ (Fig. 11). These values differ slightly from accepted PA_0 , but fall inside the PA_0 errors (Table 7). From long-slit observations, Mulder (1995) obtained $PA_{\text{dyn}} = 285\text{--}290^\circ$ for stellar component in the galactic disk as a whole. This value differs certainly from our measurements at $r < 10''$.

Our H α velocity field is similar to the data of Mulder (1995), but it has no measurements inside $r < 25''$. Here the broad H α absorption line distorts the emission line profile. The absorption does not affect the [N II] emission. The [N II] velocity field reveals non-circular ionized gas motions, as is shown from the fact that PA_{dyn} turns at $r = 5\text{--}30''$. The non-circular motions most likely connected with bar-like structure at $r < 15\text{--}20''$, detected from isophotal parameters variations: a turn of PA and a peak (Fig. 11). This conclusion confirms the result by Wong & Blitz (2000) who suggest that molecular gas kinematics is consistent with radial flows in the central stellar bar ($30''$ in diameter).

Shaw et al. (1993) also considered a twist of NIR isophotes at $r < 5\text{--}7''$, which may be explained as a secondary bar effect. We must notice that the most contrast part of circumnuclear mini-spiral locates at these radii and distorts the shape of the isophotes in the HST images. This spiral structure is studied in a recent work of Elmegreen et al. (2002).

The dust lanes in the spiral appear in the HST image up to $r = 20\text{--}30''$. Thus, the deviations of PA_{dyn} of the ionized gas velocity field from PA_0 at these radii can be explained by non-circular gas motions in the mini-spirals instead of motions inside a large-scale bar as was mentioned above.

4.10. NGC 5566

The disk inclination is considerably smaller than the value of $i_0 = 80^\circ$ measured by Jungwiert et al. (1997). We found $i_0 = 64^\circ$ by means of the "spiral criterion". This value is in a good accordance with the outer isophote ellipticity (Fig. 12) and with Kent (1984) CCD-observations. The large-scale bar of $25''$ in size is elongated at $PA = 155^\circ$. Two strong spiral arms start from the bar ends. The velocity field of stars lacks significant non-circular motions as PA_{dyn} coincides with PA_0 within the errors. The stellar rotation velocity at $r = 10 - 14''$ reaches 250 km s^{-1} that corresponds to the HI rotation curve of Helou et al. (1987).

Jungwiert et al. (1997) explained the isophotal ellipticity peak and the PA turn at $r < 5''$ as secondary bar features. We disagree with this interpretation for the following reasons. First of all, the "secondary bar" and line of nodes position angles are very similar. Secondly, two symmetrically twisted spiral arms appear in the JHK⁰ residual images. Such distribution of the underlying stellar component is not characteristic for a bar (Fig. 12). And finally, a grand-design two-armed nuclear spiral is seen also in the HST residual image (Fig. 12) at these radii.

Therefore, we suggest that NGC 5566 is an ordinary barred galaxy. A circumnuclear disk ($r = 5'' - 8''$, or $500 - 750 \text{ pc}$ in linear radius) with a mini-spiral nests inside this bar. The mini-spiral is traced by dust lanes but the main part of dust clouds concentrate outside spiral arms in the NW half of HST PC2 image. The properties of the inner isophotes ($PA = 205 - 210^\circ$, $m_{\text{ax}} = 0.55$) indicate that this kiloparsec-size inner disk lies in the galactic plane.

4.11. NGC 5850

Since our NIR images have a field-of-view that is not large enough to cover the entire galaxy, we used the R-band image, from the digitized atlas of Frei et al. (1996) to determine the orientation parameters. The spiral arms are low-contrast outside the ring around large-scale bar ($r > 80''$). Higdon et al. (1998) have shown that outer spirals have a mixed (2- and 3-armed) structure. However, the orientation parameters, determined by means of the "spiral criterion", from the $m = 2$ harmonic are in good agreement with preliminary data of Friedli et al. (1996), and with kinematics of neutral hydrogen if the possible warp of HI-disk will be taking into account (Higdon et al., 1998). Since the inner isophotes have a sharp turn at $r < 10''$, Friedli et al. (1996) have assumed the existence of a secondary bar in this galaxy.

The MPFS data show that PA_{dyn} of the stellar rotation coincides with PA_0 , while in the ionized gas PA_{dyn} , in the circumnuclear region, differs, by more than $50 - 60^\circ$, from the line of nodes position angle (Fig. 13). It is interesting to note that the ionized gas PA_{dyn} almost aligns with the PA of inner isophotes. Such radial behavior of PA_{dyn} is typical for a disk inclined to the galactic plane. Nevertheless, if we assume that the gas motions are pro-

duced in the galactic plane, then they would correspond to a radial outflow from the nucleus⁴ with velocities of $50 - 70 \text{ km s}^{-1}$, without assuming any circular rotation. Such outflows are typical for Seyfert galaxies, nevertheless, no AGN or starburst-like features are observed in the optical spectrum of the galaxy nucleus (see discussion in Higdon et al., 1998). A more reasonable assumption is that the gas, at $r < 6 - 7''$, rotates in a polar plane with respect to the global galactic disk. In this case, the polar gaseous disk lies roughly in the smallest principal-plane, cross-section of the outer bar, orthogonal to the major axis of the bar as in NGC 3368 (Sect. 4.6). The hypothesis of a polar disk is supported by the fact that NGC 5850 has undergone a recent collision with the nearby galaxy NGC 5846 (Higdon et al. 1998). Through their interaction, part of the gas could be transported to polar orbits. What is the inclination of this disk to the line of sight? It is easy to show that an angle between the inner disk plane and the outer galactic disk, i , satisfies the following relation:

$$\cos i = \sin i_1 \sin i_0 \cos(PA_1 - PA_0) + \cos i_1 \cos i_0;$$

where i_1 is the angle between the line of sight and the plane perpendicular to the disk, and PA_1 is the position angle of the disk major-axis. By substituting $PA_0 = 335^\circ$, $i_0 = 37^\circ$ (Table 7), and $PA_1 = PA_{\text{dyn}} = 35^\circ$ into this expression, we predict that the disk will be polar ($i = 90^\circ \pm 5^\circ$) for $i_1 = 65 - 74^\circ$. The gas rotation curve in Fig. 13 was calculated for $i_1 = 65^\circ$.

At $r > 5''$, the gas rotation velocities may be lower than the stellar ones, but both velocities are consistent within the errors. An extrapolation of the HI rotation curve (Higdon et al., 1998) to the inner radii gives $V_{\text{rot}} = 30 - 45 \text{ km s}^{-1}$ at $r = 5'' - 8''$, in good agreement with our ionized gas measurements.

4.12. NGC 5905

Unfortunately, we have not obtained the image of the outer isophotes, extended beyond a large-scale bar at $r = 37''$ (bar size is taken from Friedli et al., 1996). Therefore, we accepted $i_0 = 40^\circ$ that was derived by van Moorsel (1982) from the HI kinematics analysis. Also we calculated $PA_0 = (130 - 5^\circ)$ from inspection of the HI isovelocity map (Fig. 8 in van Moorsel, 1982). The last value agrees perfectly with results of deep CCD-photometry by Kent (1984).

The H velocity fields of stars and ionized gas exhibit a PA_{dyn} deviations from PA_0 at $r = 1'' - 9''$, in the opposite direction with respect to the PA s of inner isophotes. Hence they should be caused by non-circular motions in the large-scale bar. The observed slower [O III] ionized gas rotation compared with the H value and the difference

⁴ Here, we use Higdon's et al. (1998) suggestion about the galaxy disk orientation, namely that its western half is closest to the observer.

of the PA_{dyn} values in these lines are most likely connected with shock fronts in the bar edges, as in the case of NGC 3786 (Sect. 4.7).

Friedli et al. (1996) showed that the turn of the inner isophotes, at $r < 10''$, is caused by a secondary bar. Nevertheless, they used an obviously wrong value of $PA_0 = 45^\circ$. It is interesting to note that a relatively small value of the ellipticity of the inner isophotes, and the coincidence of the isophotal PA with PA_0 does not allow us to explain the central structure with a secondary bar. Most probably, the twist of the central isophotes at $r = 5'' - 10''$ is caused by the transition of the surface brightness distribution character from a bar-dominated to a central prolate bulge or circumnuclear disk. This situation is similar to that of NGC 5566 (Sect. 4.10), but without introducing the mini-spirals.

4.13. NGC 6951

The orientation parameters from Table 7 agree with Perez et al. (2000) results. The ionized gas velocities, measured by them in three different positions of the slit, coincide completely with our velocity fields. However, we did not detect the two kinematic components in stellar rotation, perhaps because of the low M PFS spectral resolution, relative to that of Perez et al. (2000) long-slit data. In the star velocity field, the PA_{dyn} differs, by $5^\circ - 10^\circ$, from the PA_0 (Fig. 15). The turn of the dynamical axis is not very significant. This fact is connected with non-circular motions in the external bar, because the bar isophotes deviate in the opposite direction relative to PA_0 .

At large distances from the center, the IFP H and [N II] velocity fields are similar (Fig. 21). Nevertheless, the [N II] rotation velocities are lower than the H ones inside the circumnuclear star-forming ring at $r = 5'' - 10''$, while the IFP H and [N II] and the M PFS H PA_{dyn} variations are the same. In contrast, the M PFS [O III] velocity field exhibits more significant non-circular ionized gas motions. The dynamical axis, found from this line measurements, turns by 30° at $r < 3''$, and the rotation velocity is twice less than the H velocities. The intensity of the [O III] decreases sharply outside this region. It is possible that radial motions of high excited ionized gas, with a speed of the same order of the rotation velocities, occur here. Radial motions are connected with the outflow from an active nucleus, which has a transition type between a LINER and a Sy 2 (Perez et al., 2000). Moreover, non-thermal radio continuum image shows a jet-like feature, extended from the nucleus up to 80 pc (Saikia et al., 2002). Unfortunately, the M PFS data cannot resolve this asymmetrical structure.

There is a circumnuclear ring at $r = 5'' - 7''$, nested in the large-scale bar, which has a $r = 60''$. The turn of isophotes, in the ground-based optical images, inside $r < 6''$ was explained by Wozniak et al. (1995) with a possible secondary bar. However, Friedli et al. (1996), basing on NIR photometry, have assumed that the isophotes

distortion is caused by a complex dust and star formation regions distribution inside the central kiloparsec. The HST image resolved this ring into individual star-forming knots. The ring seems to be elliptical, but it is almost circular after deprojection onto the galactic plane (PA and of the central isophotes correspond to the outer disk orientation). Indeed, the HST high-resolution images confirm the lack of the secondary bar as an elongated stellar structure (Fig. 15).

The HST residual brightness maps reveal a multi-armed occulted spiral (Fig. 15), described in details by Perez et al. (2000). The mini-spiral is probably associated only with the distribution of gas and dust rather than with the stellar component. As it has been shown by Perez et al. (2000), the nuclear spiral structure, clearly seen in the V band, completely disappears in the H band, where the effect of dust absorption is much weaker.

Figs. 15 and 21 reveal that the position angle of the dynamical axis, calculated from the H, H, and [N II] velocity fields, at $r = 0'' - 8''$ deviates by $10^\circ - 15^\circ$ from the PA_0 . This fact proves the significant role of non-circular motions in the disk kinematics. Since there is no inner bar in this region, we can offer the following interpretation of the observed picture. A gaseous dusty disk of $6'' - 8''$ ($400 - 600$ pc) in radius is embedded into the large-scale bar. In this disk, a multi-armed spiral structure is developed and perturbs the circumnuclear gas rotation. The dynamical decoupling of this disk is also confirmed by a high central molecular-gas density (Kohno et al., 1999), and by the location of two ILRs of the large-scale bar (Perez et al., 2000).

Based on their IFP observations, Rozas et al. (2002) presented similar arguments to explain the kinematic decoupling of the inner ionized-gas disk in NGC 6951. However, they tried to interpret the gas non-circular motions in terms of an inclined disk or a dissipation of the secondary bar. In a forthcoming paper we are going to consider a detailed kinematics and circumnuclear structure of this galaxy, based on new 2D-spectroscopy data, with a sub-arcsecond angular resolution (Moiseev, private communication).

4.14. NGC 7743

A regular two-armed spiral is seen in the ground-based images, most certainly in residual images (Fig. 16). The turn of isophotes, inside $r = 50''$, was explained by Wozniak et al. (1995) as a combined influence of a bar and a triaxial bulge, with the bulge dominating at $r < 10''$. Our analysis of residual images, and behavior of the $m = 2$ Fourier harmonic shows that the bar has a smaller size and the spiral structure distorts the elliptical isophotes at $r > 20'' - 30''$. The sharp isophote twist, at $r < 3''$, can be seen as well on ground-based as on HST images (see Fig. 16). The W FPC 2 residual optical images reveal a complex multi-armed spiral (Fig. 16).

This spiral completely disappears in the near-infrared N ICM O S images. Apparently, this spiral has a dust origin (like the gaseous-dusty spiral in NGC 6951). Unfortunately, our M P F S ionized-gas velocity field, in the mini-spiral region, is uncertain. The [O III] emission line is weak and noisy. We can only conclude that at $r < 2'' - 4''$ the gas follows the stellar rotation. A region with non-circular motions is located at large distances, South from the center.

The velocity field of stars shows a regular rotation with almost constant PA_{dyn} , while the mean PA_{dyn} value differs, by $\sim 30^\circ$, from PA_0 . The deviations go in the same direction of the inner isophotes turn. Moreover the $PA_{\text{dyn}} = 300 - 310^\circ$ coincides with orientation of the inner N ICM O S isophotes. This fact is normal for an inclined rotated nuclear disk. Nevertheless, on the our ground-based and HST images this region ($r < 8''$) is not distinguish, except by the mini-spiral at $r < 4''$. It is possible that the accepted value of PA_0 is not correct. Additional observations of this galaxy focused on the large-scale gas and stellar kinematics are needed.

The stellar velocity dispersion field is noisy (Fig. 16), but it is in good accordance with the long-slit observations of Komendy (1982), concerning the values of the central velocity dispersion, and the position of the peak, shifted by $3'' - 4''$ from the photometric center.

5. Discussion

5.1. Circumnuclear morphology of the candidate double-barred galaxies

In the Table 8 we collect all structural and kinematic features which have been found in the observed galaxies. The Table contains galactic name, type in according to the RC3 catalogue, accepted distance from the HyperLeda database ($H_0 = 75 \text{ km s}^{-1} \text{ Mpc}^{-1}$), bar major-axis length and position angle⁵ and brief description of the structures at different spatial scales. The properties for one bar are given in each case because we could not confirm kinematically secondary bars in any galaxy. Usually the bars described were denoted as "primary" in references. However in NGC 3368 and NGC 3768 only nuclear dynamically decoupled bars are present (denoted as "secondary" in references), and "large-scale primary bars" are, in fact, artifacts of isophotes distorted by spiral arms (Sect. 4.6 and 4.6).

We have detected various types of deviations of the stellar and gaseous motions from the normal regular rotation in the circumnuclear regions of the galaxies observed. These types are separated below.

⁵ The estimations of a and PA from our isophotal analysis have a preliminary character. See Erwin (2003) for more certain values.

5.2. Non-circular motions in bars.

The PA_{dyn} calculated over the ionized gas velocity fields disagrees with the lines of nodes PA_0 in all galaxies where emission lines have been detected. In Sect. 4 we have shown that the central turns of ionized-gas PA_{dyn} occur in opposition to the "primary bar" isophotes independent on the orientation of the secondary bar-like structure (excluding galaxies with inner polar and counter-rotated gaseous disks, Sect. 5.4 and 5.5). We have explain such behaviours of the "dynamical axes" as non-circular gas motions (radial flows) in a large-scale bar (or a nuclear mini-bars in the case of NGC 3368 and NGC 3786) in agreement with models given in Sect. 3. In the stellar velocity fields the amplitudes of PA_{dyn} deviations are usually less than in the gaseous ones, in the half of the sample PA_{dyn} is close to the PA_0 value. In NGC 3368, NGC 3786, NGC 5905, and NGC 6951 significant (by $7 - 20^\circ$) PA_{dyn} deviations are detected. Again they are typical signatures of non-circular motions in a single-barred galaxy, or of radial motions due to elongated stellar orbits, including the case of twisted x_2 orbits.

There is an interesting case of NGC 2950, where the inner isophotes are turned by more than 50° (Fig. 7), but PA_{dyn} for the stellar component is aligned with the line of nodes. Neither the outer bar nor the inner bar-like structure have an appreciable effect on the stellar velocity field. It's possible that both disk stellar motions within the bar and the rotation of the bulge, whose contribution in this SB0 galaxy must be significant, are observed along the line of sight. Since the spectral resolution was too low to separate two dynamical components within the line of sight velocity distribution (LOSVD), the mean velocity field corresponds to circular rotation. The stellar component associated with the outer bar in NGC 2950 affects the velocity dispersion distribution, whose increase (elliptical peak of $\sim 100 \text{ km s}^{-1}$) implies a broadening of the LOSVD in the bar region (Sect. 5.6).

5.3. Embedded disks?

In the significant fraction of the galaxies the inner disks nested in the central regions of the large-scale bars are found from kinematical and morphological analysis (in NGC 470, NGC 2273, NGC 2681, NGC 5566, NGC 5905, and NGC 6951)⁶. Below we summarize the signatures indicating the inner-disk structure:

- { Photometry: an orientation of the inner isophotes agrees with an outer disk's line of nodes PA_0 .
- { Kinematics: the central PA_{dyn} of the stellar velocity field lies near the PA_0 .

⁶ Here we don't mention NGC 3945 which has a massive inner disk embedded in the bar discussed by Erwin et al. 2003. And in his last paper based on photometric data Erwin (2003) argued also an inner disk origin for the isophotal twists in NGC 470 and NGC 2273.

Table 8. Circumnuclear structure of the sample galaxies.

Name	Type (RC3)	D ¹ M pc	Bar		Circumnuclear structure				type of the feature
			a, ⁰⁰	PA,	r, ⁰⁰	r, kpc			
NGC 470	SAb	32.6	30	20	0 6	0 1:1	lopsided nuclear disk		
					8 20	1:3 3:2	gas radial motions in the bar		
NGC 2273	SBa	25.7	25	108	0 3	0 0:4	jet outflow in [O III] line		
					1 4	0:1 0:5	nuclear disk with mini-spirals		
					3 27	0:4 3:4	gas radial motions in the bar		
NGC 2681	SAB0/a	9.6	60	30	0 5	0 0:2	stellar/gaseous polar (inclined) disk		
					5 20	0:2 0:9	decoupled disk with dusty mini-spiral		
NGC 2950	SB0	18.9	40	155	{	{	{		
NGC 3368	SABab	10.6	5	125	0 2	0.1	gaseous polar disk		
					0 5	0 0:3	stars radial motions in the mini-bar		
					5 200	0:3 1:1	global gaseous disk inclined to the stellar one		
NGC 3786	SABa	36.1	6	70	2 6	0:4 1:0	gas/stars radial motions in the mini-bar		
NGC 3945	SB0	17.7	40	72	0 6	0 0:5	counter-rotated gaseous disk		
NGC 4736	SAb	4.8	18	20	0 25	0 0:6	mini-spiral structure with non-circular gas motions		
NGC 5566	SAb	19.9	20	155	0 8	0 0:8	nuclear disk with mini-spiral		
NGC 5850	SBb	34.2	80	115	0 6	0 1:0	polar gaseous disk		
NGC 5905	SBb	47.2	30	200	0 8	0 1:9	nuclear disk; gas/stars radial motions in the bar		
NGC 6951	SABbc	21.9	80	90	0 3	0 0:3	jet outflow in [O III] line		
					1 8	0:1 0:8	stars radial motions in the bar		
					3 8	0:3 0:8	nuclear disk with mini-spiral and non-circular gas motions		
					30 55	3:2 5:9	gas radial motions in the bar		
NGC 7743	SB0	24.4	30?	95	0 4	0 0:5	mini-spiral structure		
					0 8	0 8	warped (inclined) disk? Need more information		

{ Morphology: There are inner mini-spirals at corresponding distances ($r < 1$ kpc) in NGC 2273, NGC 2681, NGC 5566, and NGC 6951. An origin of the mini-spirals is not understood yet, various models are proposed (for review see Elmegreen et al., 2002; Englmaier & Shlosman, 2000). Nevertheless, a "spiral" is some disk instability developed in the relatively thin and flat layer. The mini-spirals appear also on the images of NGC 4736 and NGC 7743, though we cannot determine inner disks in these galaxies.

{ Resonances: In the case of NGC 2681 and NGC 6951 we have shown that an inner disk region is kinematically decoupled because it lies inside ILR of a global bar.

To confirm the inner disks hypothesis we tried to extract their brightness distribution in the galactic plane. For this goal we subtracted a large-scale model of galaxy as a whole from the available images. A two-dimensional model of the surface brightness distribution is needed, because barred galaxies are actually non-axisymmetric. Our

model included disk with central brightness I_d and exponential scale r_d , Sersic (1968) bulge and global bar. A two-dimensional surface distribution of the bulge brightness is characterized by three parameters: effective brightness I_e , radius r_e , and apparent ellipticity b (see equation (1) in Moriondo et al., 1998). For a bar surface brightness distribution we adopted Ferrer's ellipsoidal distribution (Binney & Tremaine, 1987) projected onto the sky plane as:

$$I(x; y) = I_b (1 - (x/a)^2 - (y/b)^2)^m$$

(the bar is aligned with the x-axis). Here a and b are bar's semi-axes, m is an integer parameter, I_b (or I_e when given in magnitudes) is central brightness. A bar's position angle PA_b must be added for an arbitrary coordinate axes orientation.

The model was calculated through the iterative technique by means of the IDL-based software GIDRA (Moiseev, 1998). As a first step we average the original image data in the ellipses with PA_0 and i_0 and calculate the first

approximation of the m_d and r_d in the disk-dominated region from the brightness profile obtained. The 2D model of the exponential disk is subtracted from the original image. The bar-dominated region of the residual images then is interactively fitted for bar's parameter determination. After removal of the 2D bar's model we accept ellipticity of the isophotes as a first approximation for bulge ellipticity b , and construct the averaged profile again. This profile is fitted by the Sersic's law. Then the cycle is repeated to refine the model. Usually 2-3 iterations are enough for the realistic model. The model-subtracted images and the accepted parameters of the models are shown in Fig. 3. We note that the profiles on the right plots of Fig. 3 are calculated by averaging all component images, these are not "classical" one-dimensional fitting! Also we have deprojected residual images to galactic plane (Fig. 3, middle column). The nuclear over-subtraction for NGC 470 relates to the atmospheric seeing limitation. The deprojected images reveal positive brightness residuals as the true circular structures around the nucleus of NGC 470 and the spiral structures in the inner round disks in NGC 2273 and NGC 5566. The case of NGC 2681 is more complex, the residual disk is elliptical in the galactic plane that can be connected with a tum of x_2 orbits inside the ILRs. Unfortunately there is no 2D kinematic information for $r = 10 - 20''$, new observational data are needed for more certain conclusion about this galaxy.

We must note that our decomposition has a preliminary character. The main conclusion is that the residual brightness distributions demonstrate disk-like morphology (includes ring-like one in NGC 470). A more complex 2D model combining together images in different bands (optical, NIR) and through different resolutions (HST plus ground-based) is required for a detailed inspection of the inner disks in barred galaxies. But such modelling is beyond the scope of our paper.

5.4. Polar (inclined) disks

The kinematic data provide evidence for inner polar disks in NGC 2681 and NGC 5850. Significant deviations (by more than 50%) of the PA_{dyn} from the line of nodes occurring in the same direction as PA of the inner isophotes are used as a main argument for this conclusion. Also a similar disk in NGC 3368 is detected on the basis of the HST morphology (dust lane corresponds to the disk's edge and etc., see Sect. 4.6 and Sil'chenko et al., 2003) because the angular resolution of our 2D spectrographs fails on this spatial scales. What is an origin of these disks? We see two possibilities.

Firstly, the disks could be formed by an accretion of external matter with specific orientation of the angular momentum, as in "classical" large-scale stable polar rings (see, for example, Amaldi & Sparke, 1994). Indeed, NGC 2681 demonstrates some spectral (widely distributed starburst) and structural (disturbed dust lanes in the central disk) features, which has been ascribed to the merging

of external gas (see Cappellari et al., 2001 and Sect. 4.4). It is possible that in NGC 3368 all ionized/neutral/molecular gas collected in the global warped disk has an external origin (Sect. 4.6 and Sil'chenko et al., 2003) that is implied by the large-scale distribution of the neutral gas in the Leo I group (Schneider, 1989). Also the morphology of the neutral gas in NGC 5850 suggests high-speed encounter with the nearby NGC 5846 (see Sect. 4.11 and Higdon et al., 1998).

From the second point of view, we must note that the polar nuclear disks in NGC 3368 and NGC 5850 are orthogonal to the bars' major axes that could not be casual. In recent years, such polar mini-disks associated with a large-scale bar or a triaxial bulge have been detected in the circumnuclear regions of several isolated galaxies, for example in NGC 2841 (Afanasyev & Sil'chenko, 1999) or NGC 4548 (Sil'chenko, 2002). It is possible that the gas in the centers of these galaxies has been moved onto the polar orbits due to bar's effect as it is offered in qualitative model by Sofue & Wakamatsu (1994). Unfortunately, a detailed numerical simulations of this process and check of its stability are absent.

It is possible that both mechanisms (an internal as well as an external ones) are working in the described galaxies. For detailed discussion on polar disks with a size of a few hundred parsecs see Sil'chenko (2002) and Corsini et al. (2003a). In the last paper a list of 15 galaxies with the nuclear polar disks has been collected and their properties were investigated. New observations and numerical simulations are needed to understand completely these galactic structures. We hope that increasing amount of the observational information about inner polar disks will stimulate new theoretical works in this field.

5.5. A counter-rotation

We have found that the ionized gas in the central kiloparsec of NGC 3945 rotates in the opposite direction with respect to the stellar disk. According to Kuijken et al. (1996), the gaseous disks in lenticular galaxies demonstrate a counter-rotation phenomenon in the 24-8% of all cases. Therefore, this is a frequent kinematic feature in early-type galaxies. This fact is probably attributable to a merger of an accreted gaseous cloud with the corresponding direction of the angular momentum (Bertola et al., 1992). Against this background, the gas counter-rotation in the center of NGC 3945, one of four S0 galaxies in our sample (see Tab. 8) and one of three ones with gaseous disks (NGC 2681, NGC 3945, and NGC 7743), comes as no surprise.

5.6. Stellar velocity dispersion appearance

Simple models of single-barred galaxies show (Miller & Smith, 1979; Vauterin & Dejonghe, 1997) that central elliptical peak in the distribution of σ must be aligned with the outer bar orientation. In our sample the el-

Fig. 3. Surface brightness decomposition for four galaxies. Left – the 2D model was removed from an original image. A solid line corresponds to the galactic major axis, center – deprojection of the residual brightnesses to a galactic plane. The gray scale (common for the left and central images) is in magnitudes. Circles mark the radius of the inner disks denoted in the Table 8 right – azimuthally averaged surface brightness profiles of the images – solid lines, and for the model's components (bulge, bar, and exponential disk) – dotted lines. The parameters of the components are also given here.

lopsidal peaks of the distributions are found in six galaxies (NGC 470, NGC 2273, NGC 2681, NGC 2950, NGC 3945, NGC 5905). As it has been shown in our previous papers (Moiseev et al., 2002; Moiseev, 2002b), over our sample the position angle of the peaks reveals strong correlation with large-scale bar major-axis PA (see Fig. 4 in Moiseev, 2002b). But there is no any correlation between the symmetry axis of the velocity dispersion and the inner isophotal orientation. So in these objects the large-scale bars determine the dynamics of the stellar component even in the regions where the photometric "inner bars" are observed.

In NGC 3786 a central drop of the stellar velocity dispersion is found (Sect. 4.7). Recently, Elm selsen et al. (2001a) and Marquez et al. (2003) have observed similar drops in the radial distributions in the central parts of some barred galaxies with AGN. These drops can be probably attributed to the "cold" (from the dynamical point of view) stellar disk embedded into the bar. Indeed, the recent self-consistent N-body simulations by Wozniak et al. (2003) show "that young stars born in the nuclear regions from dynamically cold gas have a lower velocity dispersion than the older stellar populations". Such drop was also previously observed in NGC 6951 (Perez et al.,

2000; Marquez et al., 2003) up to distances of $6-8''$ from the center (Fig. 5 in Marquez et al., 2003). Unfortunately, our map for this galaxy has smaller size (Fig. 15), so we could not detect this interesting feature of the stellar kinematics.

5.7. Molecular gas morphology

Recently Petitpas & Wilson (2002, 2003) proposed new method for resolving secondary bar's origin. They compared turns of NIR isophotes with molecular gas (CO) distributions. Namely, if NIR and CO images have similar features, it may suggest then the isophote twists are related to structures hosted by disks and not with triaxial bulges. Over our sample, we have found detailed CO maps for NGC 470 (Jogee et al., 2001), NGC 2681 (Jogee et al., 2001), NGC 2273 (Petitpas & Wilson, 2002), NGC 3368 (Sakamoto et al., 1999), NGC 4736 (Wong & Blitz, 2000), and NGC 6951 (Kohno 1999). In ve galaxies (except NGC 3368) the orientation of CO-distribution coincides with one of our NIR (or optical) images. We think that the physical reasons of this effect can be different:

- { In NGC 470, NGC 2273, and NGC 6951 the isocontours of the inner CO distribution matches the PA and σ of the outer isophotes. We suggest that molecular gas is distributed in the nuclear disks discussed above (Sect. 5.3), the spatial scales of the CO-disks and the photometric ones being also the same. Two gaseous clumps symmetric with respect to the center found by Petitpas & Wilson (2002) in NGC 2273 can be connected with bright segments of the inner mini-spiral (Fig. 3), or may correspond to the stellar and gas orbit crowding near the ILR of the primary bar (see Petitpas & Wilson, 2002).
- { In NGC 2681 and NGC 3368 the central molecular gas is connected to the inner polar disks, hence these disks are CO-rich. But in NGC 3368 the NIR isophotes cannot relate to the polar disk, because this disk is seen in a dust distribution only, not in that of the stellar component (see scheme in Fig. 18 in Sil'chenko et al., 2003).
- { And in NGC 4736 the molecular bar elongated along the stellar bar is present (see notes in Sect. 4.9).

So, the molecular gas morphology does not contradict to existence of the structures found in this paper (nuclear coplanar and polar disks).

5.8. Where are the secondary bars?

The circum nuclear (of a few kiloparsec in size) regions in all candidate double-barred galaxies of our sample (except NGC 5566) are dynamically decoupled, because the deviations of the dynamical axes relative to the lines of nodes or elliptical peaks of σ are detected on our 2D maps. Different peculiar structures (inner polar and coplanar disks, mini-spirals) were revealed. Such large fraction

of peculiar structures is not surprising, because "photometric double bars" are claimed "by definition" in barred galaxies with complex (peculiar) central regions. But we have not found any kinematic features connected with inner (secondary) bars. This fact cannot be explained by a limited angular resolution of our kinematic data, because we can surely see the nuclear minibars (without large bars) in NGC 3368 and NGC 3786. We see two possibilities to explain this fact.

Firstly, it is possible that the twist of the inner isophotes of galactic images has no connection with a dynamically decoupled inner bar. In this case the "secondary bar" is an illusive structure, and the different reasons may provide the isophotal distortion: inner disks or nuclear spirals. Indeed, Shaw et al. (1993) had constructed a model where inner twist of the stellar isophotes is triggered by a secular evolution of the gaseous component in a single-barred gas-rich galaxy. See also papers of Friedli et al. (1996), Moiseev (2001b), and Petitpas & Wilson, (2002) where various mechanisms are considered for an isophotal twist explanation.

Secondly, the kinematics of the inner bar in a double-barred galaxy differs essentially from a single-bar dynamics. In this case, the deviations of PA_{dyn} and velocity dispersion peaks must be interpreted in a different manner than in this paper. For example, in their last work Corsini et al. (2003b) have measured different pattern speeds for secondary and primary bar-like structures in NGC 2950. However, PA_{dyn} of the stellar velocity field coincides with the line of nodes (see Sect. 4.5). New self-consistent models of barred galaxies must be used to investigate this phenomenon.

Of course, selection effects must be kept in mind because our sample is small: we studied only 13 galaxies from Moiseev's (2001b) list, or only 6 objects from 50 "photometrically confirmed" double-barred galaxies of Erwin (2003). However, our sample contains the most "classical" double-barred objects with the strong twist of the inner isophotes (NGC 2681, NGC 5850 etc.).

Nevertheless, the existing samples of double-barred candidates must be revised. First of all, additional 2D kinematics data (panoramic spectroscopy, HI and CO interferometric radio observations) must be acquired for studying any dynamical decoupling of the circum nuclear regions. We hope that our paper is only the first small cautious step in this promising way.

6. Conclusion

The analysis of the morphology and kinematics of 13 double-barred galaxy candidates observed by means of the panoramic spectroscopy at the SAO RAS 6m telescope is presented in this paper. We tried to collect the maximum possible information from observed 2D distributions of the optical and NIR surface brightness and kinematic properties. For this goal, panoramic spectroscopy observations were carried out at the 6m telescope. The ionized gas and stars velocity fields and velocity dispersion field were con-

structed from these observations. The rotation curves and radial variations of the dynamical axis position angle were calculated. The analysis of the morphology of the galaxies was done by means of isophotes analysis of NIR and optical ground-based and HST archival images.

We suggest that candidate double-barred galaxies are, in fact, galaxies with very different circumnuclear structure. It is necessary to note that the majority of the observed, morphological and kinematic features in our sample galaxies may be explained without the secondary bar hypothesis. Three cases of inner polar disks, one counter-rotated gaseous disk and seven nuclear disks (with as well as without mini-spirals) nested in the large-scale bars were found in this work. However, we think that the observational data presented here, the 2D kinematics first of all, will be useful to proponents as well as to opponents of the secondary bar hypothesis. Doubtlessly the models of such galaxies must explain all their observed kinematic properties.

Acknowledgements. We would like to thank Olga Silchenko, Victor Afanasiev, Lilia Shaliapina and Enrico Corsini for their interest and numerous discussions. We also thank the referee, Glen Petitpas for careful reading and useful comments. This research has made use of the NASA/IPAC Extragalactic Database (NED), which is operated by the Jet Propulsion Laboratory, California Institute of Technology, under contract with the National Aeronautics and Space Administration. Also HyperLeda database and data from Canadian Astronomy Data Center (CADC) were used. CADC is operated by the Herzberg Institute of Astrophysics, National Research Council of Canada. The authors would like to thank all the staff of the Observatorio Astronómico Nacional, in San Pedro Martir, Mexico for their assistance during the NIR observations. This work was partially supported by the RFBR grant No. 03-02-06070mas and by the Russian Federal program "Astronomy".

References

Aguerri, J.A.L., Debattista, V.P., Corsini, E.M., 2003, *MNRAS*, 338, 465
 Afanasiev, V.L., Dodonov, S.N., Moiseev, A.V., 2001, in *Stellar dynamics: from classic to modern*, eds. Osipkov L.P., Nukiforov I.I., Saint Petersburg, 103
 Afanasiev, V.L., Mikhailov, V.P., Shapovalova, A.I., 1998, *Astron. Astrophys. Trans*, 16, 257
 Afanasiev, V.L. & Shapovalova, A.I., 1981, *Astrophysics*, 17, 221
 Afanasiev, V.L. & Shapovalova, A.I., 1996, *ASP Conf. Ser.*, 91, 221
 Afanasiev, V.L., & Silchenko, O.K., 1999, *AJ*, 117, 1725
 Amoldi, M. & Sparke, L.S., 1994, *AJ*, 107, 958
 Bames, E.I., & Sellwood, J.A., 2003, *AJ*, 125, 1164
 Begelman, K.G., 1989, *A & A*, 223, 47
 Bender, R. & Moellenho, C., 1987, *A & A*, 177, 71
 Bertola, F., Buson, L.M., Zeilinger, W.W., 1992, *ApJ*, 401, L79
 Bertola, F., Cinzano, P., Corsini, E.M., Rix, H.-W., Zeilinger, W.W., 1995, *ApJ*, 448, L13
 Binney, J., & Tremaine, S., 1987, *Galactic Dynamics*: Princeton
 Buta, R., 1986, *ApJS*, 61, 609

Buta, R., & Crocker, D.A., 1993, *AJ*, 105, 1344
 Cappellari, M., Bertola, F., Burstein, D., et al., 2001, *ApJ*, 551, 197
 Chevalier, R.A., & Furenlid, I., 1978, *AJ*, 225, 67
 Corsini, E.M., Pizzella, A., Coccato L., Bertola F., 2003a, *A & A*, 408, 873
 Corsini, E.M., Debattista, V.P., Aguerri, J.A.L., 2003b, *ApJ*, accepted
 Cruz-Gonzalez, L., Carrasco, L., Ruiz, E., et al., 1994, *Rev. Mex. Astron. Astrof.*, 29, 197
 de Vaucouleurs, G., 1975, *ApJS*, 29, 193
 Dodonov, S.N., Vlasjuk, V.V., Drabek, S.V., 1995, *Interferometer Fabry-Perot: user manual*, N Arkhiv
 Ferruit, P., Wilson, A.S., Mulchaey, J., 2000, *ApJS*, 128, 139
 Englmaier, P., & Shlosman, I., 2000, *ApJ*, 528, 677
 Erwin, P., 2003, *A & A*, submitted
 Erwin, P. & Sparke, L.S., 1999, *ApJ*, 521, L37
 Erwin, P. & Sparke, L.S., 2002, *AJ*, 124, 65
 Erwin, P. & Sparke, L.S., 2003, *ApJS*, 146, 299
 Erwin, P., Vega Beltran J.C., Beckman J., 2001, *ASP Conf. Proc.*, 249, 171 (astro-ph/0112056)
 Erwin, P., Vega Beltran J.C., Graham, A.W., Beckman, J.E., 2003, *ApJ*, accepted
 Elmegreen, D.M., Elmegreen, B.G., Eberwein, K.S., 2002, *ApJ*, 564, 234
 Emmellen, E., 2002, astro-ph/0202522
 Emmellen, E., Geusard, D., Combes, F., et al., 2001a, *A & A*, 368, 52
 Emmellen, E., Geusard, D., Friedli, D., Combes, F., 2001b, *Astrop. and Space Science (Suppl.)*, 277, 455
 Emmellen, E., & Friedli, D., 2000, *ASP Conf. Ser.*, 197, 51, (astro-ph/9910260)
 Fridman, A.M., Afanasiev, V.L., Dodonov, S.N. et al., 2003, submitted to *A & A*
 Frei, Z., Guhathakurta, P., Gunn, J.E., Tyson, J.A., 1996, *AJ*, 111, 174
 Friedli, D., & Martinet, L., 1993, *A & A*, 277, 27
 Friedli, D., Wozniak, H., Rieke, M., Martinet, L., Bartschi, P., 1996, *A & A S*, 118, 461
 Hagen-Thom, V.A. & Reshetnikov, V.P., 1997, *A & A*, 319, 430
 Heller, C., Shlosman, I., Englmaier, P., 2001, *ApJ*, 553, 661
 Helou, G., Salpeter, E.E., Terzian, Y., 1987, *AJ*, 87, 1443
 Heraudeau, P., Simien, F., Moubon, G., Pagnuel, P., 2001, *A & A S*, 136, 509
 Higdon, J., Buta, R., Purcell, G.B., 1998, *AJ*, 115, 80
 Garcia-Gomez, C., & Athanassoula, E., 1991, *A & A S*, 89, 159
 Jogee, S., Baker, A.J., Sakamoto, K., Scoville, N.Z., Kenney, J.D.P., *ASP Conf. Proc.*, 2001, 249, 612 (astro-ph/0201209)
 Jungwiert, B., Combes, F., Axon, D.J., 1997, *A & A S*, 125, 479
 Junquera, S., & Combes, F., 1996, *A & A*, 312, 703
 Kent, S.M., 1984, *ApJS*, 56, 105
 Kohno, K., Kawabe, R., Vila-Vilaro, B., 1999, *ApJ*, 511, 157
 Komendy, J., 1982, *ApJ*, 257, 75
 Kuijken, K., Fisher, D., Merrield, M.R., 1996, *MNRAS*, 283, 543
 Laine, S., Shlosman, I., Knäpen, J.H., Pelletier R.F., 2002, *ApJ*, 567, 97
 Lindblad, P.O., *A & A Rev.*, 1999, 9, 221
 Lyakhovich, V.V., Fridman, A.M., Khoruzhii, O.V., Pavlov, A.I., 1997, *Astron. Reports*, 41, 447
 Maciejewski, W., & Sparke, L.S., 2000, *MNRAS*, 313, 745
 Maciejewski, W., Teuben, J., Sparke, L.S., Stone, J.M., 2002, *MNRAS*, 329, 502

- Marquez, I., Masegosa, J., Durret, F., et al., 2003, *A & A*, 409, 459
- Miller R. H., & Smith, B. F., 1979, *ApJ*, 227, 785
- Moiseev, A. V., 1998, preprint of the SAO RAS, 134, 1
- Moiseev, A. V., 2000, *A & A*, 363, 843
- Moiseev, A. V., 2001a, *Bull. Spec. Astrophys. Obs.*, 51, 11 (astro-ph/0111219)
- Moiseev, A. V., 2001b, *Bull. Spec. Astrophys. Obs.*, 51, 140 (astro-ph/0111220)
- Moiseev, A. V., 2002a, *Bull. Spec. Astrophys. Obs.*, 54, 74, (astro-ph/0211104)
- Moiseev, A. V., 2002b, *Astronomy Letters*, 28, (astro-ph/0211105)
- Moiseev, A. V. & Mustsevoi, V. V., 2000, *Astro. Letter.*, 26, 665 (astro-ph/0011225)
- Moiseev, A. V., Valdes, J.R., Chavushan, V.O., 2002, *ASP Conf. Ser.*, 282, 261 (astro-ph/0202192)
- Monnet, G., Bacon, R., Emmellen, E., 1992, *A & A*, 253, 366
- Moriondo, G., Giovanardi, C., Hunt, L.K., 1998, *A & A S*, 130, 81
- Mulchaey, J.S., Regan, M.W., Kundu, A., 1997, *ApJS*, 110, 299
- Mulder, P.S., 1995, *A & A*, 303, 57
- Petitpas, G.R., & Wilson, C.D., 2002, *ApJ*, 575, 814
- Petitpas, G.R., & Wilson, C.D., 2003, *ApJ*, 587, 649
- Perez, E., Marquez, I., Durret, F., et al., 2000, *A & A*, 353, 893
- Pfenninger, D., & Norman, C.A., 1990, *ApJ*, 363, 391
- Richter, O.-G., & Sancisi, R., 1994, *A & A*, 290, L9
- Rozas, M., Relano, M., Zurita, A., Beckman, J.E., 2002, *A & A*, 386, 42
- Saikia, D.J., Phookun, B., Pedlar, A., Kohno, K., 2002, *A & A*, 383, 98
- Sakamoto, K., Okumura, S.K., Ishizuki, S., Scoville, N.Z., 1999, *ApJS*, 124, 403
- Schinnerer, E., Maciejewski, W., Scoville, N., Moustakas, L.A., 2002, *ApJ*, 575, 826
- Schneider, S.E., 1989, *ApJ*, 343, 94
- Sersic, J.-L. 1968, *Atlas de Galaxias Australes* (Cordoba: Obs. Astron.)
- Shalyapina, L.V., Moiseev, A.V., Yakovleva, V.A., *Astronomy Letters*, 28, 443, (astro-ph/0206397)
- Shaw, M.A., Combes, F., Axon, D.J., Wright, G.S., 1993, *A & A*, 273, 31
- Shlosman, I., Frank, J., Begeman, M.C., 1989, *Nature*, 338, 45
- Shlosman, I., & Heller, C., 2002, *ApJ*, 565, 921
- Sil'chenko, O.K., 2002, *Astro. Letter.*, 28, 207
- Sil'chenko, O.K., Moiseev, A.V., Afanasiev, V.L., Chavushyan V.H., Valdes J.R., 2003, *ApJ*, 591, 185
- Sofue, Y., Wakamatsu, K.I., Taniguchi, Y., Nakai, N., 1993, *PASJ*, 45, 43
- Sofue, Y., & Wakamatsu, K.I., 1994, *AJ*, 107, 1018
- Tonry, J., & Davis, M., *AJ*, 84, 1511
- Tumbull, A.J., Bridges, A.J., Carter, D., 1997, *MNRAS*, 307, 967
- van Driel W., & Buta R.J., 1993, *A & A*, 245, 1991
- van Moorsel, G., 1982, *A & A*, 107, 66
- Vauterin, P., & Dejonghe, H., 1997, *MNRAS*, 286, 812
- Vega Beltran, J.C., Pizzella, A., Corsini, E.M., et al., 2001, *A & A*, 374, 394
- Wong, T., & Blitz, L., 2000, *ApJ*, 540, 771
- Wozniak, H., Friedli, D., Martinet, L., Martin, P., Bartschi, P., 1995, *A & A S*, 111, 115
- Wozniak, H., 2000, *ASP Conf. Ser.*, 197, 75, (astro-ph/9910007)
- Wozniak, H., Combes, F., Emmellen, E., Friedli, D., 2003, *A & A*, 409, 469
- Zasov, A.V. & Khoperskov, A.V., 2002, *Astronomy Reports*, 46, 173

Fig. 4. NGC 470. The left panel shows the results of MPFS-observations. Here the top row contains the continuum images, the velocity field of the stars, and the map of their velocity dispersion. In the middle row the emission line image, the velocity field of the ionized gas and the map of ionized gas velocity dispersion are given. At the bottom the radial dependences of the rotation velocity and the PA of the dynamical axis are shown. The dotted line marks the line of nodes (PA_0). At the right panel the left column contains large-scale image, while the right column contains the image of the nuclear region. The logarithm-scaled images with the corresponding isophotes are presented in the top row of the panel. The residual brightness distributions are plotted in the middle row. The thick dotted line shows maximum of $m = 2$ harmonic. At the bottom the PA and ellipticity of the isophotes are plotted. The horizontal dotted line corresponds to the PA_0 value, and the vertical dotted line (in the left plot) marks the radial range, which is zoomed at the right plots.

Fig. 5. The same as Fig. 4 for NGC 2273

Fig. 6. The same as Fig. 4 for NGC 2681

Fig. 7. The same as Fig. 4 for NGC 2950

Fig. 8. The same as Fig. 4 for NGC 3368

Fig. 9. The same as Fig. 4 for NGC 3786

Fig. 10. The same as Fig. 4 for NGC 3945

Fig. 11. The same as Fig. 4 for NGC 4736

Fig. 12. The same as Fig. 4 for NGC 5566

Fig. 13. The same as Fig. 4 for NGC 5850

Fig. 14. The same as Fig. 4 for NGC 5950

Fig. 15. The same as Fig. 4 for NGC 6951

Fig. 16. The same as Fig. 4 for NGC 7743

Fig. 17. IFP observations in the H α line. left { NGC 470. At the top continuum and H α images plotted in a square-root scale. The cross marks the dynamical center. At the bottom the velocity field with isoveLOCITIES is shown. The thick black contour corresponds to the systemic velocity, while the thin contours indicate line of sight velocities in steps of 50 km s $^{-1}$. And the last plot shows the rotation curve and the kinematic position angles. Here the dotted line marks the PA_0 value. There is ghost from bright stars locate in position (20 $^{\circ}$; 35 $^{\circ}$). right { same for NGC 2273

Fig. 18. NGC 3368. IFP observations in the [N II] (left) and H α lines (right). The dotted line correspond to the Position Angle of the gaseous disk 170 $^{\circ}$ (see texts).

Fig. 19. IFP observations of NGC 3945 in the [N II] line.

Fig. 20. NGC 4736. IFP observations in the [N II] (left) and H α lines (right).

Fig. 21. NGC 6951. IFP observations with IFP in the [N II] (left) and H α lines (right).

This figure "fig3.jpg" is available in "jpg" format from:

<http://arxiv.org/ps/astro-ph/0311271v1>

This figure "fig4.jpg" is available in "jpg" format from:

<http://arxiv.org/ps/astro-ph/0311271v1>

This figure "fig5.jpg" is available in "jpg" format from:

<http://arxiv.org/ps/astro-ph/0311271v1>

This figure "fig6.jpg" is available in "jpg" format from:

<http://arxiv.org/ps/astro-ph/0311271v1>

This figure "fig7.jpg" is available in "jpg" format from:

<http://arxiv.org/ps/astro-ph/0311271v1>

This figure "fig8.jpg" is available in "jpg" format from:

<http://arxiv.org/ps/astro-ph/0311271v1>

This figure "fig9.jpg" is available in "jpg" format from:

<http://arxiv.org/ps/astro-ph/0311271v1>

This figure "fig10.jpg" is available in "jpg" format from:

<http://arxiv.org/ps/astro-ph/0311271v1>

This figure "fig11.jpg" is available in "jpg" format from:

<http://arxiv.org/ps/astro-ph/0311271v1>

This figure "fig12.jpg" is available in "jpg" format from:

<http://arxiv.org/ps/astro-ph/0311271v1>

This figure "fig13.jpg" is available in "jpg" format from:

<http://arxiv.org/ps/astro-ph/0311271v1>

This figure "fig14.jpg" is available in "jpg" format from:

<http://arxiv.org/ps/astro-ph/0311271v1>

This figure "fig15.jpg" is available in "jpg" format from:

<http://arxiv.org/ps/astro-ph/0311271v1>

This figure "fig16.jpg" is available in "jpg" format from:

<http://arxiv.org/ps/astro-ph/0311271v1>

This figure "fig17.jpg" is available in "jpg" format from:

<http://arxiv.org/ps/astro-ph/0311271v1>

This figure "fig18.jpg" is available in "jpg" format from:

<http://arxiv.org/ps/astro-ph/0311271v1>

This figure "fig19.jpg" is available in "jpg" format from:

<http://arxiv.org/ps/astro-ph/0311271v1>

This figure "fig20.jpg" is available in "jpg" format from:

<http://arxiv.org/ps/astro-ph/0311271v1>

This figure "fig21.jpg" is available in "jpg" format from:

<http://arxiv.org/ps/astro-ph/0311271v1>